ACSNANO

www.acsnano.org

REVIEW

Challenges and Prospects of Bio-Inspired and Multifunctional Transparent Substrates and Barrier Layers for Optoelectronics

Sajad Haghanifar, Anthony J. Galante, and Paul W. Leu*

Cite This: https://dx.doi.org/10.1021/acsnano.0c06452

Read Online

ACCESS | Metrics & More | Article Recommendations

ABSTRACT: **Bio-inspiration and advances in micro/nanomanufacturing processes have enabled the design and fabrication of micro/nanostructures on optoelectronic substrates and barrier layers to create a variety of functionalities. In this review article, we summarize research progress in multifunctional transparent substrates and barrier layers while discussing future challenges and prospects. We discuss different optoelectronic device configurations, sources of bio-inspiration, photon management properties, wetting properties, multifunctionality, functionality durability, and device durability, as well as choice of materials for optoelectronic substrates and barrier layers. These engineered surfaces may be used for various optoelectronic devices such as touch panels, solar modules, displays, and mobile devices in traditional rigid forms as well as emerging flexible versions.**

KEYWORDS: *superomniphobicity, flexible substrates, antireflection, light scattering, pressure stability, optoelectronics, stain resistance, condensation resistance, mechanical durability*

INTRODUCTION

Over the past decade, there has been a proliferation in optoelectronic devices such as solar panels, displays, tablets, phones, touch panels, light-emitting diodes (LEDs), and sensors. An essential component in these devices is the substrate or barrier layer, which needs to provide high optical performance, protect the device from the environment, as well as provide for multifunctionality. The substrate or barrier layer can be rigid, such as glass, or flexible, such as plastics and papers.

Figure 1 shows various optolectronic substrates and barrier layers as well as sources of bio-inspiration for achieving different material properties and functionalities. This review article summarizes sources of bio-inspiration and recent advances in micro/nanomanufacturing. Future challenges and possibilities for using optolectronic substrates and barrier layers in modern optoelectronic devices are discussed.

This review article consists of four main sections. In the Introduction, we provide a brief overview of optoelectronic substrates and barrier layers. We briefly discuss optoelectronic device configurations, source of bio-inspiration, photon management properties, wetting properties and multifunctionality, durability considerations, as well as choice of materials. In the second section, we discuss photon management properties, which includes broadband and broad angle antireflection as well as haze management. In the third section, we discuss wetting properties and various functionalities. Desirable functionalities for optoelectronics include antisoiling, self-cleaning, stain resistance, antifogging, and anti-icing. Finally, in the last section, we discuss the durability of optoelectronic devices with regard to device durability, stability in the presence of different stressors, property and functionality durability, and durability strategies.

Optoelectronic Device Configurations. Figure 2 shows three different configurations of optoelectronic devices: (a) superstrate, (b) substrate, and (c) bifacial. This classification is based on which side the light passes through to reach the device layer. In the superstrate configuration (Figure 2a), light passes through the transparent substrate. Devices in the superstrate configuration are deposited on a transparent substrate, which acts as a supporting material. On the other side of the device, there is an encapsulation layer, which may

Received: August 1, 2020
Accepted: November 11, 2020

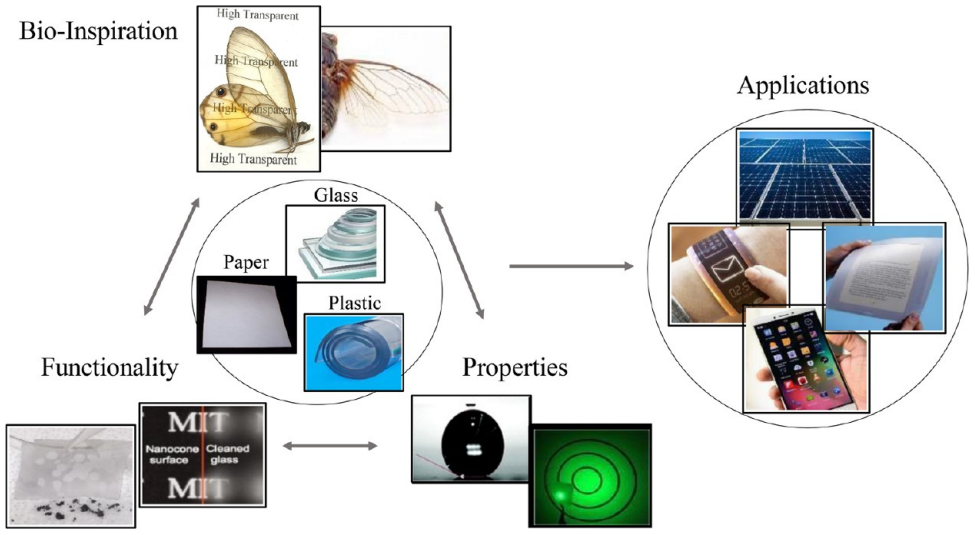

Figure 1. Glass, plastics, and papers are the most common optoelectronic substrates and barrier layers. Inspired by nature, many functionalities such as self-cleaning,[1] antifogging,[2] as well as stain resistance[3] can be created for these substrates or barrier layers. Surfaces in nature such as the moth eye,[4] wings of cicada,[5] and glasswing butterfly wing[6] provide bio-inspiration. Micro/nanostructures provide controlled optical properties such as light scattering[7,8] and tunable wetting properties.[1] Multifunctional optoelectronic substrates and barrier layers can be used in many devices such as smart phones, e-paper, solar modules, and flexible devices. Cicada wing image reprinted from ref 5. Copyright 2015 American Chemical Society. Antifogging image reprinted from ref 9. Copyright 2012 American Chemical Society. Light scattering image reprinted with permission from ref 8. Copyright 2017 The Optical Society.

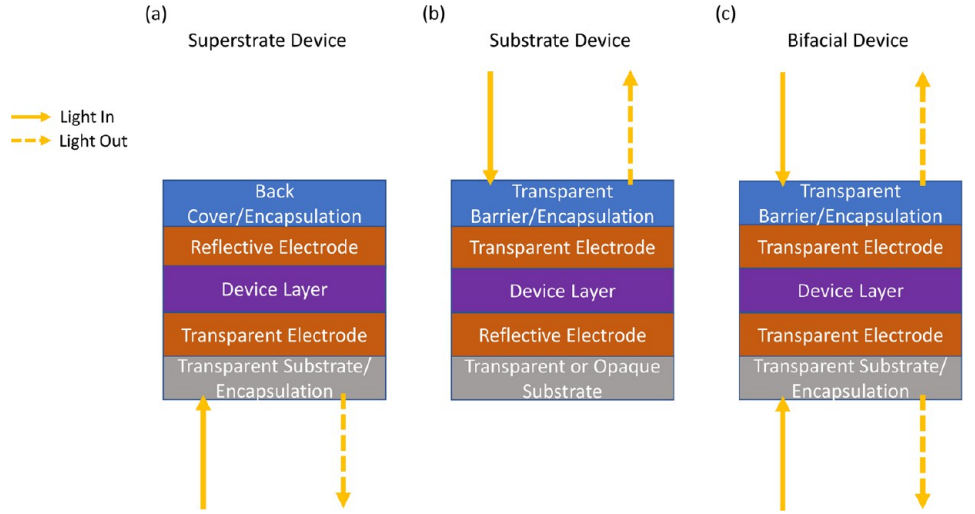

Figure 2. Schematic of the (a) superstrate, (b) substrate and (c) bifacial layer configurations for optoelectronic devices.

be opaque. In the substrate configuration (Figure 2b), light passes into or out of the cell through the transparent barrier film on the other side of the substrate. The optical properties of the substrate are not important, and thus a wide variety of substrates including opaque materials such as metal foils or stainless steel may be used. In this configuration, the device requires an encapsulant and transparent barrier layer on the top of the device. In the bifacial configuration (Figure 2c), the substrate layer and top barrier layer must both be transparent for light to pass through to or from the device in both directions. This review paper focuses on describing substrates and barrier films where optical transparency is important. That is, this paper discusses the substrate in the superstrate configuration, the barrier layer in the substrate configuration, as well as both the substrate and barrier layer in the bifacial configuration.

Bio-Inspiration. Natural species have surfaces with specific topography and functionalities that may help them survive in their environment. Textures found in nature provide for various optical properties such as transparency, antireflection, light absorption, and antihazing, as well as various desired functionalities from micro/nanoscale features that are related to liquid repellency such as antisoiling, self-cleaning, stain resistance, antifogging, and anti-icing. Biological surfaces have inspired research to understand how the physical and chemical properties of different surfaces provide for such functionalities and guided the development of various synthetic surfaces.

Photon Management Properties. Optoelectronic substrates and barrier layers must have high transparency to allow photons to either pass into or out of the active layer in the device with high efficiency. To increase transparency, reflection from the surface−air interface needs to be minimized. The antireflection may be desired across a wide range of

https://dx.doi.org/10.1021/acsnano.0c06452
ACS Nano XXXX, XXX, XXX−XXX

wavelengths, which is referred to as broadband antireflection. Additionally, the antireflection may be needed over a broad range of incidence angles, which is referred to as broad angle antireflection, or over all angles, which is referred to as omnidirectional antireflection. Broadband and broad angle or omnidirectional antireflection properties are essential for many optoelectronic substrates and barrier layers.

Light scattering is also important for several optoelectronic devices such as solar cells[10] and light-emitting diodes (LEDs),[11] where the efficiency of these devices can be enhanced by increasing light scattering. Haze is a parameter for quantifying the light scattering and will be discussed in detail in the haze management section. While many applications such as displays, need low light scattering, to achieve high clarity,[12−15] high haze can increase the power conversion efficiency or extraction efficiency of solar cells and LEDs, respectively.

Wetting Properties and Multifunctionality. Functionalities such as antisoiling, self-cleaning, and antifogging provide value to optolectronic devices as these functionalities help the device perform with high efficiency in different environmental conditions. A surface with liquid repellency results in droplets balling up on the surface and easily rolling off as opposed to droplets soaking, penetrating, or leaving behind a wet residual on the surface that may interfere with optical performance. Antisoiling surfaces reduce the adhesion of dust or other airborne particulates onto the surface, which negatively affect the optical performance of the device. Dust and dirt particles can be removed from self-cleaning surfaces with the use of water or solvent. Many applications require stain resistance functionality. Various liquids leave behind a stain or change in color after they dry, which can reduce transmission. Stain resistance functionality helps to prevent this negative effect. This functionality can also prevent fingerprint marks, for example, from remaining on the surface (also referred to as smudge resistance). Antifogging surfaces inhibit condensation formation so that visibility is not hindered even in humid environments. Anti-icing surfaces reduce the formation of ice, which can also inhibit visibility. These functionalities can be achieved by changing the micro/nanostructure and chemistry of the surface and are often correlated with the wetting behavior of the surface.

Durability of Optoelectronic Devices. Optoelectronic substrates and barrier layers are important for the long-term durability of the optoelectronic device. The substrate and barrier film is part of the encapsulation, where it acts as a protective layer between the device and the environment. Oxygen and water vapor must be prevented from diffusing through the substrate and interacting with and degrading the optoelectronic device. In addition to this essential function, the various properties and functionalities of the optoelectronic device must be maintained in the presence of various stressors, such as abrasion, elevated temperature, liquid droplet impact, and particulate impact. Various strategies are being researched to enhance the durability of optoelectronic substrates and barrier layers.

Choice of Materials. The three materials that are typically considered for optoelectronic substrates and barrier layers are glass, plastics, and paper. The most common material is glass due to its high transmission, reasonable cost, and excellent barrier properties. Common types of glass include soda lime and fused silica. Recent demands for lighter weight and flexibility for flexible optoelectronic applications have led to research into thinner glass. This not only helps reduce the overall weight of the device but may also enable flexibility as the bending stiffness is proportional to the thickness of the material to the third power.[16]

Plastics may also be integrated into flexible optoelectronics due to their flexibility. Plastics have acceptable mechanical durability, light weight, and low price in combination with good optical performance and may be manufactured scalably and with low cost by methods such as roll-to-roll manufacturing. However, their low melting point provides challenges in their incorporation into optoelectronic devices, and their poor barrier properties result in challenges in long-term durability. Also, issues with the recycling of plastics is a major concern and a hindrance for their wide usage.

Transparent paper has attracted much attention from both industry and researchers as a flexible substrate for optoelectronics. Paper is an environmentally sustainable material that can be made with scalable roll-to-roll manufacturing processes.[17] It is lightweight, low cost, and flexible and can be engineered to be transparent. Paper is mainly made of cellulose fibers up to 50 μm in diameter and several millimeters in length where the microfibrils consist of nanofibrils with a diameter of a few nanometers.[18] Paper's roughness and microstructure are typically what makes it opaque. In recent years, researchers have demonstrated transparent paper for optoelectronics by reducing the presence of pores and surface roughness.[19−36] Transparent paper can be incorporated in photovoltaics as a substrate[37−46] or antireflection coating.[47,48] Also, paper may be integrated with transparent conductive electrodes[28,42,49−70] and used in optoelectronics such as organic light-emitting diodes (OLEDs),[71−81] displays, and touch screens.[49,82] However, major challenges exist for paper in demonstrating scalability of manufacturing for transparency, abrasion resistance, and barrier properties. Creating functionalities related to liquid repellency also present a challenge.

PHOTON MANAGEMENT

Optoelectronic substrates and barrier films must allow light to transmit through the material with high efficiency so that light can either couple into or out of the active layers of the device. Optical losses may occur due to reflection or absorption of light. For non-absorbing materials, the transparency and reflection must sum to 100%, and thus, maximizing transparency is the same as minimizing reflection. Optoelectronic substrates and barrier layers consist of two interfaces where reflection may occur: between the substrate (or barrier layer) and the air and between the substrate (or barrier layer) and the device material. Antireflection is important for increasing power conversion efficiencies in solar modules, extraction efficiencies in displays or LEDs, and the sensitivity or responsivity of sensors.

Substrates and barrier layers are typically used with a quarter wavelength thickness antireflection layer coating that reduces reflection losses at the interfaces using destructive interference.[83] This antireflection coating consists of an intermediate thin film layer with an index of refraction that is the geometric mean of the materials on both sides n_0 and n_2, $n_1 = \sqrt{n_0 n_2}$, and thickness $d = \frac{\lambda}{4n_1}$, where λ is the wavelength of light. A single layer antireflection coating can suppress reflection to 0% at normal incidence at a particular wavelength by destructive interference. However, antireflection is often desired over a broad range of wavelengths. Multilayer antireflection coatings

https://dx.doi.org/10.1021/acsnano.0c06452
ACS Nano XXXX, XXX, XXX−XXX

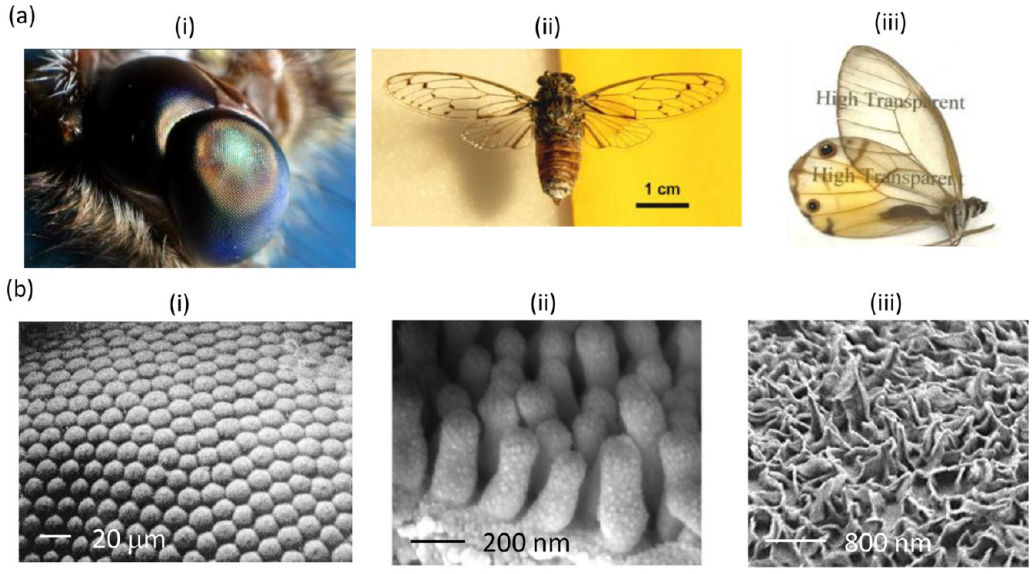

Figure 3. Antireflection surfaces in nature. (a) Optical and (b) scanning electron microscope (SEM) images of a (i) moth eye,[4] (ii) transparent cicada wing,[87] and (iii) transparent glasswing butterfly. Moth eye images reprinted with permission from ref 4. Copyright 2011 The Royal Society of Chemistry. Cicada images reproduced with permission from ref 87. Copyright 2014 AIP Publishing.

may be used, but the destructive interference effects of each layer in the system need to be considered to suppress reflection to close to 0% across a wider spectral range.[84]

Also, broad angle antireflection over a wide range of incidence angles or omnidirectional antireflection over all possible incidence angles is often desirable. This is important for displays where a wide viewing angle is desirable. In addition, this is relevant for solar modules due to the movement of the sun through the sky and the fixed nature of most solar module installations. The property of reducing reflection across a wide variety of wavelengths is referred to as broadband antireflection. The property of reducing reflection over a broad range of incidence angles is called broadband antireflection and over all incidence angles is called omnidirectional antireflection.

Another important optical property is optical haze. The American Society for Testing and Materials (ASTM) standard D1003[85] defines the haze factor as the percentage of scattered light as a function of wavelength (λ):

$$H(\lambda) = \left[\frac{\text{scattered transmission}(\lambda)}{\text{total transmission}(\lambda)}\right] \times 100\% \quad (1)$$

The scattered transmission is the transmitted light that deviates from the incident beam direction greater than 2.5°. The total transmission is equal to all of the transmission that passes through the material, which is the sum of the direct transmission (light that deviates less than or equal to 2.5° from the incident light direction) and the scattered transmission (light that deviates greater than 2.5° from the incident light direction).

Depending on the application, high or low optical haze is desired. For photovoltaics, high transparency and high haze substrates can increase absorption in the solar cell by enhancing the light path length inside the active layer.[37] LEDs also benefit from increased haze as this leads to increased extraction efficiency. On the other hand, low optical haze is of high importance for displays and touch screens due to the importance of higher clarity of images and text viewed.[2,86]

Many antireflecting surfaces can be found in nature. Figure 3 shows (a) optical and (b) scanning electron microscope (SEM) images of a (i) moth eye,[4] (ii) cicada wing,[87] and (iii) glasswing butterfly wing. Moths eyes are well-known for their antireflection properties.[88−90] Moth eye surfaces consist of hexagonal close-packed nanostructures that are roughly 200 nm tall with 300 nm pitch. These structures act as an effective continuous refractive index gradient between the air and the surface to provide for better antireflection. This antireflection enables insects to see better under low light conditions or at night.[91] In addition to moth eyes, various insect wings, such as that of the glasswing butterfly,[92,93] hawk moth,[94] and cicada,[87,95] exhibit antireflection properties. Nanopillars of random size and high aspect ratio cover the transparent sections of the wings. In the case of the glasswing butterfly, the random distribution of height and width of the pillars provides for omnidirectional antireflection.[6] The antireflection properties of insect wings make it more difficult for predators to spot the insect.

The surfaces of these natural surfaces consist of nanostructures that are smaller than relevant optical wavelengths. Modeling the interaction of light with these nanostructures can involve methods such as rigorous coupled mode analysis (Fourier modal method), finite element method, or finite-difference time-domain method.[96] Effective medium approximations can also be used where the nanostructures are modeled as layers of composite materials, where each layer has an effective index of refraction based on averaging the indices of refraction in that layer. This approximation allows one to solve Maxwell's equations analytically using the transfer matrix method.[97]

Researchers have pursued two main approaches for creating subwavelength nanostructured antireflecting surfaces. The first strategy consists of creating subwavelength porous and patterned structures where the effective refractive index is reduced by decreasing the volume fraction of the solid in the layer. These structures function like a medium where the

https://dx.doi.org/10.1021/acsnano.0c06452
ACS Nano XXXX, XXX, XXX−XXX

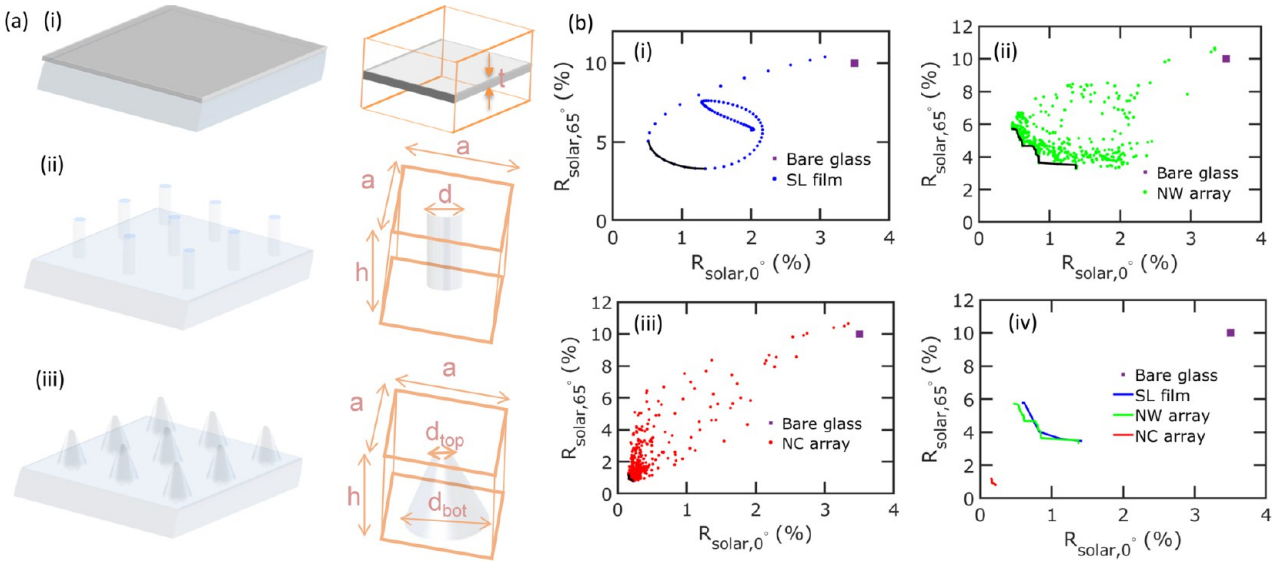

Figure 4. (a) Schematic and (b) scatter plots for (i) single thin film layer, (ii) nanowire array, and (iii) nanocone arrays. (b) (iv) Comparison of Pareto frontier of three systems in a single plot. Reprinted with permission from ref 98. Copyright 2020 The Optical Society.

effective index of refraction can be tuned by adjusting the solid fraction. These structures perform comparably to a single layer film with the ideal index of refraction,[98] but this approach is often used because durable materials with an appropriately low index of refraction may not exist.

The second strategy to reduce reflection, proposed by Rayleigh[99] and seen in the natural surfaces described above, is to gradually change the refractive index between the two materials at the interface. Han *et al.* recently reviewed several nanostructure arrays with these properties such as nanocones, nanograss, nanowires, nanoholes, and nanopyramids.[100] These antireflection structures can be fabricated by a variety of different methods such as dry etching, wet etching, multistep etching, and colloidal lithography.[101−103] Nanostructures based on the moth eye have been demonstrated, showing broadband antireflectivity.[104−106] Random nanostructures inspired by glasswing butterfly can also be utilized to reduce the reflection of light at high incidence angles.[2,6]

Broadband and Broad Angle Antireflection. Both nanowires[107] and nanocones[108] have been evaluated for solar top glass sheets, which require broadband and broad angle antireflection. For example, it has been shown that by fabricating nanowire arrays on both sides of a glass substrate, normal reflection can be reduced to 0.97% in the wavelength range of 425−1000 nm.[107] Nanocone arrays have been investigated by several research groups. Different fabrication processes such as self-assembly,[109] metal dewetting,[110] and lithography[9] have been used to fabricate nanocones in glass.

Recently, we used machine learning and optimization together with optical simulations to study the broadband and omnidirectional performance limits of three common antireflection structures including single layer films, nanowire arrays, and nanocone arrays.[98] In this work, we calculated the integrated reflection over the solar spectrum by

$$R_{\text{solar}} = \frac{\int b_s(\lambda) R(\lambda) \mathrm{d}\lambda}{\int b_s(\lambda) \mathrm{d}\lambda} \tag{2}$$

where $R(\lambda)$ is the reflection spectrum, $b_s(\lambda)$ is the photon flux density of the AM1.5 global solar spectrum,[111] and λ is the wavelength. The reflection spectrum was assessed at normal incidence angle ($R_{\text{solar},0°}$) and 65° incidence angle ($R_{\text{solar},65°}$).

We searched for solutions to the optimization problem

$$\min_{x \in \mathcal{X}} R_{\text{solar},0°}(\mathbf{x}),\ R_{\text{solar},65°}(\mathbf{x}) \tag{3}$$

where $\mathcal{X}$ is the space of all possible design parameters. We used the finite-difference time-domain method for simulations.[112]

For a single antireflection layer, only one parameter can be adjusted: the thickness of the antireflection layer t, as shown in Figure 4a(i). In this work, we assumed that the material of the single layer has the ideal wavelength-independent refraction index of $n_1 = 1.21$, which is the geometric mean of refraction indices of air, $n_0 = 1$, and fused silica glass, $n_2 = 1.46$. Figure 4a(ii) shows the NW array system, which can be defined by three parameters: pitch (a), height (h), and diameter (d). Figure 4a(iii) shows nanocone arrays as defined by the four variables, pitch (a), height (h), top diameter (d_{top}), and bottom diameter (d_{bot}). The nanowires and nanocones are made of the same glass as the underlying layer with the same refraction index at each wavelength.

The results of the simulations of the systems based on machine learning optimization are shown in Figure 4b. In these plots, the x-axis is $R_{\text{solar},0°}$ and the y-axis is $R_{\text{solar},65°}$. As shown in Figure 4b(i,ii), the performance of single layer thin films and nanowire arrays is similar. However, nanocone arrays show near perfect broadband and omnidirectional antireflection (Figure 4b(iii)). The purple box in each plot shows the performance of bare glass. Figure 4b(iv) compares the performance of the three systems and shows the advantage of nanocone arrays over nanowire arrays or single layer films. Nanocone arrays exhibit $R_{\text{solar},0°} = 0.15\%$ with corresponding $R_{\text{solar},65°} = 1.25\%$ or minimum $R_{\text{solar},65°} = 0.78\%$ with corresponding $R_{\text{solar},0°} = 0.23\%$. Effective medium analysis of near optimal nanocone arrays showed that nanocones that grade the refraction index smoothly and minimize the discontinuity between the bottom of the nanocone arrays and the top surface of the glass result in the best antireflection performance.

https://dx.doi.org/10.1021/acsnano.0c06452
ACS Nano XXXX, XXX, XXX−XXX

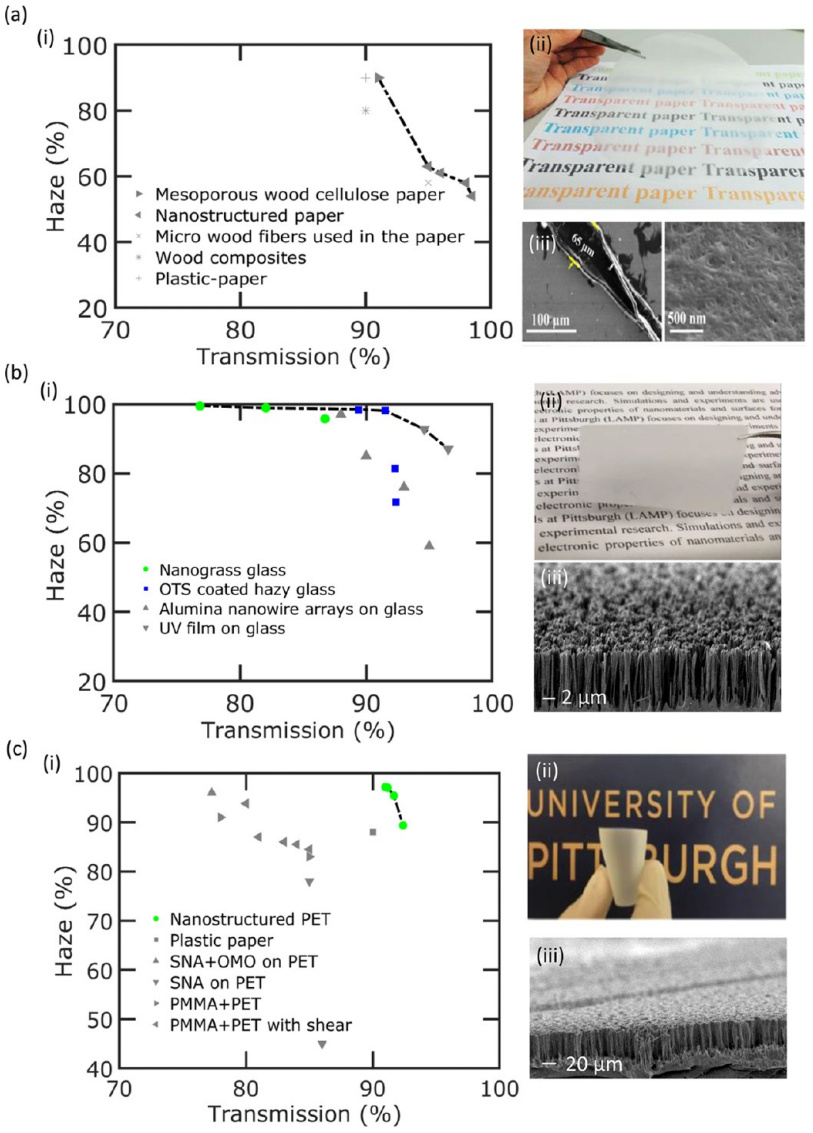

Figure 5. High transparency, high haze results for optical (a) paper, (b) glass, and (c) plastic. For (a) (i) paper, the plot includes mesoporous wood cellulose paper,[120] nanostructured paper,[37] microwood fiber in nanofiber paper,[118] wood composites,[121] and plastic−paper hybrids.[71] (b) (i) Nanograss glass with[1] and without[8] OTS coating, as well as the aggregated alumina nanowire arrays on glass[122] and imprinted PDMS on glass.[123] (c) (i) Nanograss PET,[7] as well as plastic−paper,[71] silica nanoparticle array on PET,[124] and doped poly(methyl methacrylate) (PMMA)/poly(ethylene terephthalate) (PET) without[125] and with shear.[126] Dashed lines show the Pareto frontier. Also shown are (ii) optical and (iii) SEM images of high transparency, high haze (a) paper,[37] (b) glass,[8] and (c) plastics.[7] Paper images reprinted from ref 37. Copyright 2014 American Chemical Society. Glass images reprinted with permission from ref 8. Copyright 2017 The Optical Society. Plastic images reprinted with permission from ref 7. Copyright 2018 IOP Publishing.

Haze Management. High transparency and low haze is essential for high clarity in touch screens and display applications. Antireflection coatings, as discussed in the previous section, are a practical solution to increase the transparency as well as the clarity. Surface roughness needs to be controlled in order to avoid light scattering.[2] Examples of high transparency, low haze optical substrates, and barrier layers were provided in the previous section, such as optimized nanocone arrays on glass substrates.

On the other hand, high haze has been shown to increase light absorption in the active region of solar cells.[113,114] Transmission and haze tend to be inversely proportional,[115] where increasing haze tends to decrease transparency and *vice versa*. Therefore, achieving high transparency, high haze substrates or barrier layers with values more than 80% has been challenging.

Figure 5 highlights recent work on high transparency, high haze results for (a) optical paper, (b) glass, and (c) plastic substrates and barrier layers. The total transmission and haze (at 550 nm) is plotted in (i) in each of these subfigures. For each material, the best performing data as defined by Pareto optimality are plotted. A datapoint is considered Pareto optimal or Pareto efficient if there are no other datapoints with both higher transparency and haze. In each subfigure for (a) paper, (b) glass, and (c) plastic, (ii) optical and (iii) SEM images of high haze and high transparency materials are shown.

Until recently, there were no reports on optical substrates or barrier layers with transparency over about 90% and haze more than 20%.[21,113,114,116,117] In 2014, Fang *et al.* reported a

https://dx.doi.org/10.1021/acsnano.0c06452
ACS Nano XXXX, XXX, XXX−XXX

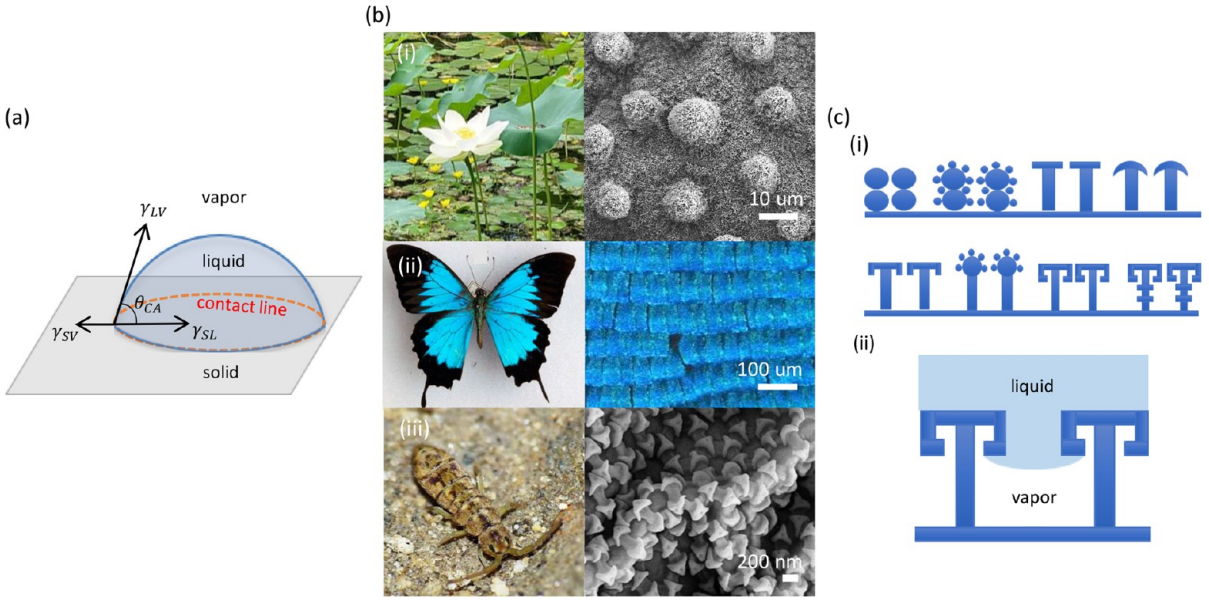

Figure 6. (a) Schematic of the three phase system (solid, liquid, and vapor) showing a static contact angle along with the surface tension interfaces at the contact line. (b) Optical and SEM images of surfaces from nature that demonstrate interesting wetting properties including (i) *Nelumbo nucifera* (sacred lotus), (ii) *Papilio ulysses* (Ulysses butterfly), and (iii) *Isotomorus palustris* (springtail). (c) (i) Examples of re-entrant structures (left to right) (top row) include microspheres, microspheres with nanospheres, microhoodoos, mushroom pillars (bottom row) serif T or doubly re-entrant microposts, nanosphere re-entrant microposts, triply nano-re-entrant microposts, and triply hierarchical nano-re-entrant microposts. (c) (ii) Schematic of a Cassie–Baxter wetting for triply nano-re-entrant microposts. Butterfly image reproduced with permission from ref 144. Copyright 2006 Journal of Experimental Biology. Springtail image credited to Lucarelli under Creative Commons license.

transparent paper based on wood fibers, with ultrahigh transparency of ≈96% as well as high optical haze (≈60%).[118] By integrating an organic solar cell with this ultrahigh transparency, high haze substrate, the power conversion efficiency (PCE) increased from 5.34 to 5.88%.[118] Afterward, they also reported the fabrication of transparent paper with haze that could be tuned from 18 to 60% by vacuum filtration.[37] In addition, in 2016, Yao *et al.* reported high transparency (more than 85%) and high haze (more than 90%) plastic–paper substrates by roll-to-roll compatible fabrication methods.[71] They showed that this substrate increases the current efficiency of an OLED by 35–40%, and the power conversion efficiency for thin film solar cells can be increased by 15%.[71] Zhu *et al.* demonstrated wood/polymer composites and demonstrated the combination of more than 90% transparency and 80% haze, which increased the efficiency of a GaAs solar cell by 18%.[119] Figure 5a(i) compares a variety of high transparency, high haze papers demonstrated, such as cellulose paper made of mesoporous wood,[120] nanofiber (and microfiber) paper,[118] wood composites,[121] nanostructured paper,[37] and plastic–paper hybrids.[71] Figure 5a shows an (ii) optical and (iii) SEM image of high transparency and high haze paper fabricated by nanostructured wood microfibers.[37] Most work on both high haze and high transparency optoelectronic substrates or barrier films have focused on paper and wood composites.

There have been few reports on high transparency and high haze glass. This has included glass with aggregated alumina nanowire arrays[122] and imprinted polydimethylsiloxane (PDMS) on glass, which showed 94.6% transparency and 92.7% haze.[123] Recently, we reported the fabrication of nanograss on glass,[1,8] which provides transparency and haze both over 90%. We used maskless reactive ion etching for fabrication of nanograss structures on fused silica glass. We showed that the optical properties of the glass substrate can be controlled by adjusting the height of the nanograss. Shorter nanograss provides better antireflection, and longer height nanograss increases the optical haze.

We also coated the nanograss structures with octadecyltrichlorosilane (OTS) to improve the hydrophobicity and show self-cleaning functionality.[1] The optical properties of nanograss glass did not change significantly with OTS coating. Figure 5b(i) shows the optical performance of nanograss glass with green circles and OTS-coated nanograss glass with blue squares. In order to compare the performance of our high transparency, high haze glass substrates, we plotted the data for optoelectronic glass substrates with the best optical properties in literature with gray color. Aggregated alumina nanowire arrays[122] and imprinted PDMS on glass[123] showed a significant optical performance improvement compared to that of other glass. As shown in Figure 5b(i), two of the green circles (nanograss glass) and two of blue squares (OTS-coated nanograss glass) are on the Pareto frontier, plotted with the dashed line. The details of the fabrication process and the dimensions of the nanograss glass and OTS-coated nanograss glass are described elsewhere.[1,8] Figure 5b shows (ii) optical and (iii) SEM images of our high transparency and high haze nanograss glass.[8]

The nanograss structure can also be made on plastic.[7] Similar to glass, the optical properties can be tuned by controlling the height of the nanograss. We have reported the fabrication of high transparency, high haze flexible plastics.[7] Figure 5c(i) shows the optical performance of the best plastic substrates reported in the literature (gray markers) as well as the performance of our high transparency high haze plastic substrates, plotted with green circles. The literature data

https://dx.doi.org/10.1021/acsnano.0c06452
ACS Nano XXXX, XXX, XXX–XXX

plotted includes plastic−papers,[71] poly(ethylene terephthalate) (PET) coated with silica nanoparticles,[124] and doped poly(methyl methacrylate) (PMMA)/PET without[125] and with shear.[126] As shown in Figure 5c(i), the Pareto line consists of only nanograss PET substrates with different height of the nanograss. Figure 5c shows (ii) optical and (iii) SEM images of our high transparency and high haze plastic.[7]

WETTING PROPERTIES AND MULTIFUNCTIONAL SURFACES

A variety of functionalities are desirable for optoelectronic substrates and barrier films related to maintaining their optical properties after exposure to various liquids or particulates. These functionalities are often closely correlated to the wetting properties of the surface and include antisoiling, self-cleaning, stain resistance, antifogging, and anti-icing. Other functionalities such as antibacterial[127] and antivirofouling[128] may also be of interest.

Surfaces may be engineered to promote various wetting states such as Cassie−Baxter and Wenzel states, which may be applied to water, oils, as well as a host of other liquids. Superhydrophobic surfaces are defined as substrates that strongly repel water with static contact angles more than 150° and hysteresis less than 10°. This type of wetting may be achieved from a metastable Cassie−Baxter wetting state.[129−131] These types of surfaces demonstrate their functionalities by maintaining an air barrier to prevent liquids from infiltrating or contaminants from adhering. Literature has also adapted the nomenclature with the prefixes oleo-, amphi-, and omni- to classify the wettability of oils, all Newtonian liquids, and all types of liquids, respectively. For example, superoleophobic surfaces demonstrate static contact angles more than 150° and hysteresis less than 10° for oils.

In contrast, superhydrophilic and superoleophilic substrates show low water and oil static contact angles, respectively, of generally less than 10° and high hysteresis from a Wenzel wetting state. Superhydrophilic/superoleophilic substrates may be helpful for applications such as oil−water separation, self-cleaning, and antifogging. These types of surfaces demonstrate these functionalities by creating a high energy liquid barrier to prevent infiltrating liquids or the adhesion of contaminants. In comparison, superhydrophobic/superoleophobic surfaces maintain an air barrier to minimize the potential contact area between the substrate and infiltrating liquids or contaminants. Most of the research in recent years has focused on the development of superhydrophobic/superoleophobic substrates due to the performance of these substrates. Surface wetting properties will first be explained in order to fully discuss these mechanisms.

Surface wettability is composed of a three phase system between solid, liquid and vapor (gas), where all three meet at the three-phase contact line. A static contact angle is formed once the contact line is motionless from reaching an equilibrium of tangential forces caused by the interfacial surface tensions. Figure 6a(i) shows a schematic of a droplet at equilibrium. Tangential surface tension forces acting along the solid−vapor, solid−liquid, and liquid−vapor interfaces are represented by γ_{SV}, γ_{SL}, and γ_{LV}, respectively.

Young was credited for describing the wetting contact angle of a completely smooth surface in contact with a liquid. The intrinsic contact angle of the surface, θ_Y is described in terms of the interfacial energies involved in the three phase (surface, liquid, vapor) system such that[132]

$$\cos\theta_Y = \frac{\gamma_{SV} - \gamma_{SL}}{\gamma_{LV}} \tag{4}$$

However, Young's equation is unable to explain the observation of naturally occurring superhydrophobic surfaces. The force balance phenomenon that results in superhydrophobic repellency occurs when sufficient air is trapped between a liquid and a surface that causes a spherical droplet to form as the thermodynamic energy on the surface is minimized.

Further surface analyses determined that wetting properties were dependent on surface morphology, spawning the development of Wenzel and Cassie−Baxter equations.[133,134] Wenzel noted that roughness increases the true surface area and added a roughness factor coefficient, r, to Young's equation in order to describe the apparent contact angle of a liquid θ_W on a rough surface by[133]

$$\cos\theta_W = r\cos\theta_Y \tag{5}$$

where r is the ratio of the actual rough surface area to the projected area. In the Wenzel model, the liquid completely wets the surface and fills all the voids in the rough surface. The inherent wetting behavior of the surface can be hydrophobic or hydrophilic and is based on the Young's contact angle. Since r is always larger than 1, roughness will further enhance the inherent wetting behavior when a surface is in a Wenzel state.

Later on, Cassie and Baxter proposed a model to describe the apparent contact angle when the surface morphology induces air pockets that make parts of the surface energetically unfavorable to be wet by liquid.[134] Ultimately, the equation is derived from considering a composite interface between the surface and the entrapped air, where the entrapped air is considered to be a fully liquid repellent surface layer. The apparent contact angle of a composite surface made partly of entrapped air θ_{CB} can be expressed as

$$\cos\theta_{CB} = f_1\cos\theta_{Y_1} + f_2\theta_{Y_2} \tag{6}$$

$$= f_1\cos\theta_{Y_1} + f_1 - 1 \tag{7}$$

$$= f_1(\cos\theta_{Y_1} + 1) - 1 \tag{8}$$

where f_1 is the fraction of the surface area that is in contact with the liquid. $f_1 + f_2 = 1$ and $\theta_{Y_2} = 180°$ for air. Typically, a Wenzel state shows higher surface to liquid adhesion, whereas a Cassie−Baxter state shows lower adhesion at the solid−liquid interface. The above-mentioned contact angles are determined solely by the region at the contact line, independent of pressure, gravity, drop size, defects, and other external factors.[135]

Wettability studies have further characterized the dynamic wetting of fabricated surfaces with the advancing contact angle, receding contact angle, contact angle hysteresis, and the transition state between Wenzel and Cassie−Baxter states.[136−138] The advancing contact angle is the angle produced in the course of being wetted; the receding angle is the contact angle where the surface has already been wetted and is in the course of being dewetted. The advancing angle is always larger than or equal to the receding angle and the contact angle hysteresis is the advancing contact angle minus the receding contact angle. The contact angle hysteresis describes the tendency of a droplet to roll off the surface when tilted and is a strong indication of the total solid−liquid interfacial area. In a physical sense, the contact angle hysteresis

https://dx.doi.org/10.1021/acsnano.0c06452
ACS Nano XXXX, XXX, XXX−XXX

is a measure of the energy dissipated while a liquid droplet moves along a surface.[139]

The transition from a Cassie−Baxter to Wenzel state occurs when water enters the air pockets of the surface and this transition is described by the Gibbs surface free energy barrier. Calculations of the global minimum Gibbs surface free energy barrier of the interface system can predict which wetting state is energetically favorable and are important for designing stable, super-repellent surfaces.[136,140,141] Furthermore, the four typical wetting states (Young, Cassie−Baxter, transition, and Wenzel) have been reported for different surface tension liquids (*i.e.*, oil), as well as different surrounding media (*i.e.*, underwater).[142,143]

Nature has inspired researchers to achieve different wettability properties and desirable functionalities by fabricating micro- and nanostructures that mimic those found on natural surfaces.[145−149] *Nelumbo nucifera*, or the lotus plant, is a famous example of a natural superhydrophobic surface. The lotus leaf utilizes simultaneous microscale convex cell papilla and nanoscale texturing from low surface energy epicuticular wax crystals that stabilize a Cassie−Baxter wetting state, even under the impact of rainfall.[127,150,151] The wax crystals are derived from long hydrocarbon chains with 20−60 carbon atoms that are inherently hydrophobic.[152,153]

Butterflies offer not only a variety of interesting colors but also waterproofing functionality in their wings.[154,155] Their colors come from appropriately scaled nanostructures for reflecting wildly diverse colors to intimidate predators, camouflage, communicate between other butterflies, and attract mates (Figure 6b(ii)).[144] Butterfly wings also demonstrate anisotropic liquid repellency from overlapping, nanogrooved microscales for stability during flight and self-cleaning in moist environments.[156] The *Morpho aega* butterfly wings were shown to be capable of reversible pinning and rolling droplet behavior due to the direction of flexible nanotips on ridging nanogrooves in overlapping microscales.[157]

Smaller organisms offer an impressive spectrum of nanoscale applications, including arguably some of the most repellent exoskeleton structures found in nature. An organism that has developed impressive surface technology is a subclass of tiny soil arthropods called springtail (Collembola), as shown in Figure 6b(iii). Different species of springtail grow highly ordered, overhanging cuticular layers of complex geometries that repel lower surface tension liquids to help them thrive in harsher soil environments.[158] Their surfaces are composed of a lamellar chitin skeleton, structural proteins, and a topmost envelope of lipids.[150,159] The overhanging cuticles are grown at a length scale and curvature that effectively stabilize a Cassie−Baxter wetting state even while immersed under elevated pressures.[141,159] Scientists have used these fascinating discoveries from nature to further influence and support the development of functional, repellent surfaces.

Based on lessons from nature, common fabrication methods for creating repellent surfaces include small length scale roughening techniques and the use of lower surface energy materials.[160−162] Sufficiently low surface tension materials are needed in order to repel lower surface tension liquids.[163] The free energy of a surface determines its wetting and is determined by the constitution and configuration of the atomic groups comprising the surface.[164] The surface energy of atomic bonds decreases in the following order: $-CH_2 > -CH_3 > -CF_2 > -CF_2H > -CF_3$.[164,165] Surface tension is further reduced in the presence of longer hydrocarbon or fluorocarbon chains. Fabrication of super-repellent surfaces using perfluorinated compounds (PFCs) or long fluorine chain molecules ($-CF_x$, $-CF_xH$) and roughening techniques are in abundance with impressive results.[162,166−168] However, the use of PFCs bring undesirable human and environmental toxicology risks.[169−173] Therefore, it is essential for future work to consider techniques with nonfluorinated materials for practical applications.[174,175]

Surfaces that repel low surface tension liquids are feasible with the use of complex, re-entrant geometries that enable repellency without the need for fluorination. Techniques for fabricating stable, superoleophobic surfaces use a low surface energy layer, roughened micro/nanostructures, and re-entrant surface curvature.[163,176,177] At appropriate angles and length scales, the overhang of re-entrant surface geometry creates net traction in the upward direction which drives the liquid−air interface to recede to the top edge of the microstructures in a three-phase system.[163,177,178] Nosonovsky used Lagrangian optimization to show that, given a surface with re-entrant nanoroughness on top of micron asperities and a stable advancing liquid at the solid−liquid interface, there exists a local Gibbs surface free energy minima based on the liquid−air interface surface tension component and its principal radii of curvature.[178] The principal radii of curvature are the two radii, R_1 and R_2, that describe the curvature of the liquid−air interface by $1/R_1 + 1/R_2$. Therefore, hiearchical roughness and re-entrant curvature were shown to provide metastable equilibrium states of liquid pinning and stabilize a Cassie−Baxter composite interface.[177,178] The stability of a Cassie−Baxter state on hiearchically rough, re-entrant surfaces has further been demonstrated and modeled with different structures, including woven fabrics,[179] textured fabrics,[180] microsphere arrays,[181] roughened pillars,[181] microhoodoos,[176] mushroom and serif T nanostructures,[182,183] doubly nano-re-entrant microposts,[184] doubly nano-re-entrant microarrays,[185] and triply nano-re-entrant microposts.[186] Figure 6c(i) shows examples of multiple re-entrant structure strategies for robust Cassie−Baxter wetting.

Multireentrant, hiearchical structures such as doubly/triply nano-re-entrant microposts/arrays maximize the liquid−air interface and the principal radii of curvature, which achieves a local energy minima for Cassie−Baxter repellency. Furthermore, increasing the number of re-entrant curvatures across various length scales enhances Cassie−Baxter wetting repellency and stability by extending the sites for local energy minima to occur. Figure 6c(ii) shows the shape of the liquid and vapor phase of a Cassie−Baxter wetting state for triply nano-re-entrant micro posts.

Theoretically, given the system is in a Cassie−Baxter state, any surface may demonstrate superphobicity of an intrinsically wetting liquid $\theta_Y = 0°$ if the fractional surface−liquid interface area is below 6%.[184] Feasibility is difficult in practice because re-entrant structures typically require precise instrumentation and multiple fabrication steps; however, exceptional repellency using intrinsically wetting materials has been achieved with repeating nanoscale re-entrant micro posts and micro arrays.[184−186] This work is important for utilizing surface wetting properties for desirable functionalities without the use of toxic or environmentally harmful materials, such as long chain fluorocarbons.

Antisoiling and Self-Cleaning. Antisoiling and self-cleaning functionalities are strongly related to each other as well as wettability properties. Antisoiling refers to the ability of

https://dx.doi.org/10.1021/acsnano.0c06452
ACS Nano XXXX, XXX, XXX−XXX

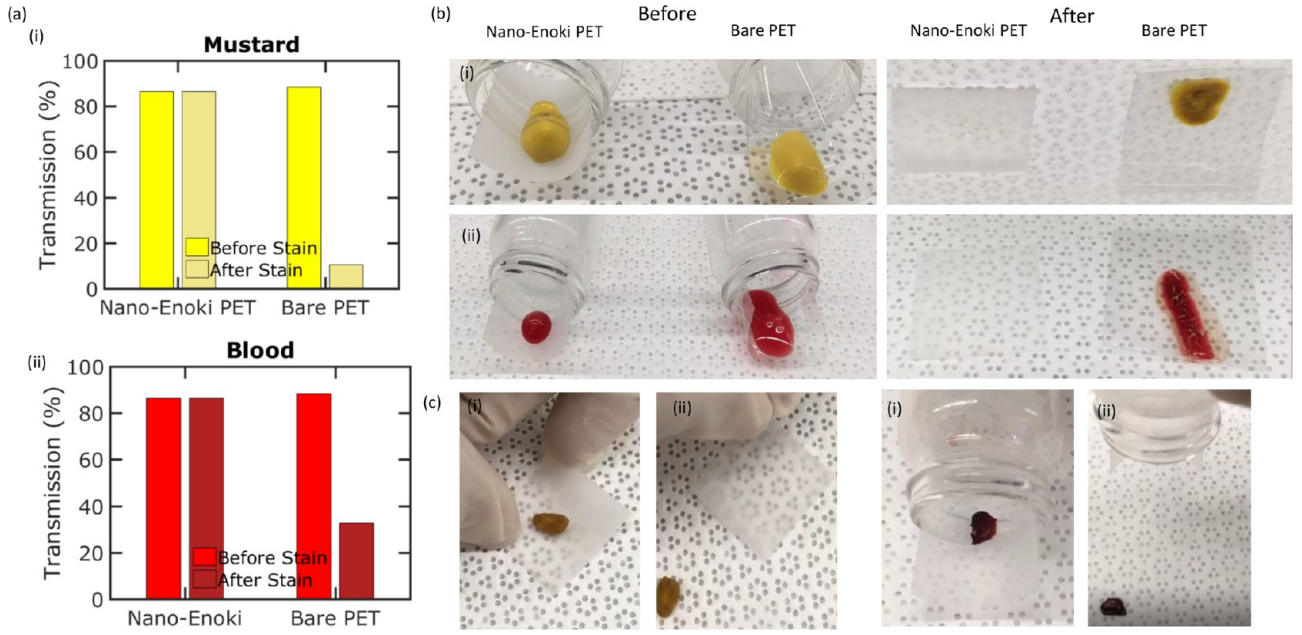

Figure 7. Stain resistance functionality of nanoenoki PET substrates. (a) Transparency at 550 nm wavelength for bare and nanoenoki PET, before and after staining of (i) mustard and (ii) blood droplets before and after evaporation. (b) Optical images of (i) mustard and (ii) blood on nanoenoki and bare PET. (c) Droplet flaking off the tilted nanoenoki PET for dried (i) mustard and (ii) blood. Reproduced with permission from ref 195. Copyright 2019 The Royal Society of Chemistry.

a surface to resist adhesion from various particulates, which may reduce transmission. Self-cleaning refers to the ability of a surface to easily remove particulates on the surface with the application of water, solvent, or some external stimuli. These two functionalities are often studied hand-in-hand since better antisoiling leads to easier self-cleaning.

Both antisoiling and self-cleaning functionalities may be achieved by reducing the fraction of surface area in contact with the particulate, which can be accomplished by roughening the surface at length scales smaller than particulates such as the nanoscale. These functionalities are thus often seen with superhydrophilic or superhydrophobic surfaces depending on whether high surface energy or low surface energy surfaces are used, respectively.[187]

Kirschner and Brennan[188] reviewed multiple bio-inspired antisoiling strategies, including chemical-, physical-, and stimuli-responsive ones. While chemical- and stimuli-responsive strategies are more applicable for organisms or biomaterials, nature inspired physical strategies, such as mollusk shells, where the structure of the surface plays a critical role on reducing the adhesion of particles on the surface, are more useful for designing antisoiling systems. A study on 36 mollusk species found that low fractal dimension, high skewness of roughness and waviness, high isotropy, and low mean surface roughness were correlated with lower antisoiling.[189]

Bahattab et al.[190] reported nanoporous SiO_2 antireflection films prepared by sol−gel process. The fabricated samples were exposed to standard Arizona test dust as well as outdoor exposure, and cleaned by an electrical fan, that demonstrated antisoiling functionality. The relative transmission loss due to outdoor exposure was reported to be 13% for the coated sample, whereas for bare glass, this loss was reported to be 19%.

Several reports in the literature of self-cleaning behavior by superhydrophilic and superhydrophobic surfaces can be found.[191] Superhydrophilic surfaces provide self-cleaning when water forms a thin layer that carries away particulates. In contrast, superhydrophobic surfaces depend on liquid repellency, where a slightly tilted surface causes water droplets to easily roll away while removing dust or dirt particles. This type of self-cleaning ability has been recognized on the lotus leaf, so it is known widely as the lotus effect.[192,193] The rough surface of the leaf reduces the adhesive force between particle and the surface, and when the droplet rolls across the surface, particles stick to the droplet instead of the surface, and thus leave a clean area behind. In this way, superhydrophobic surfaces can be cleaned from particulates.

The self-cleaning effect of removing particulates for both superhydrophilic and superhydrophobic surfaces typically require the presence of water. However, rain is not common in dry environments where sunshine is available for most hours of a day and is a great location for installing solar panels. There is thus great interest in the use of dew droplets.[194]

Stain Resistance. There are a limited number of research reports on stain resistance for optoelectronic substrates and barrier films. Antigraffiti technology has wide usage in large-scale applications, where transparency and wetting behavior are simultaneously important. Antigraffiti coatings have different forms including transparent and self-adherent polymer films, polymeric paints and self-cleaning ceramic coatings. Research to find alternatives to traditional antigraffiti coatings are currently in progress.[196] Stain-resistant materials must not only be super-repellent toward a range of liquids but also be able to repel the residue of liquids after dehydration and solidification. Many liquids leave a residual stain after drying, which may reduce or change the optical properties of the substrate or barrier layer.

Recently, we reported on the fabrication of nanoenoki mushroom-like structures on a flexible plastic substrate that demonstrated stain resistance functionality and repelled various liquids including mustard and blood in both liquid

https://dx.doi.org/10.1021/acsnano.0c06452
ACS Nano XXXX, XXX, XXX−XXX

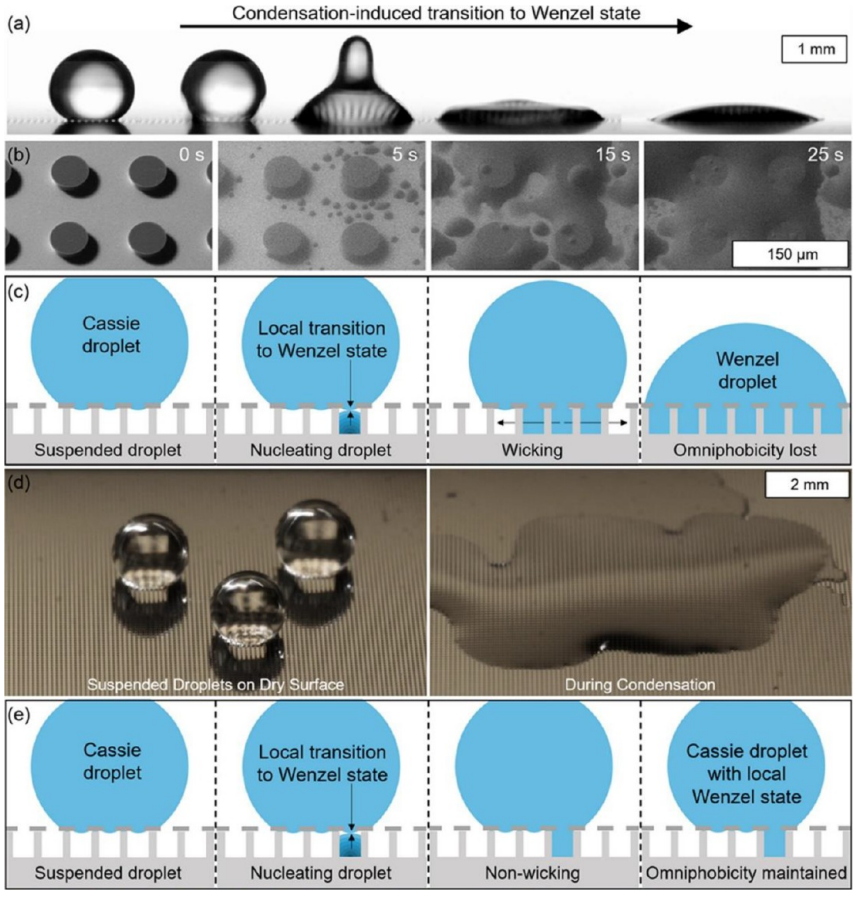

Figure 8. Condensation failure of superhydrophobic surfaces. (a) Transition of a water droplet on re-entrant structure from Cassie−Baxter state to Wenzel state due to condensation. (b) SEM images of nucleation and growth of water droplet during condensation on the reentrant structures. (c) Schematic of transition from a Cassie−Baxter state to a Wenzel state during condensation. (d) Optical images of water droplets on reentrant pillars before and after condensation on a wicking substrate. (e) Schematic of nonwicking structures that block the growth of water nucleates.[146] Reprinted from ref 146. Copyright 2018 American Chemical Society.

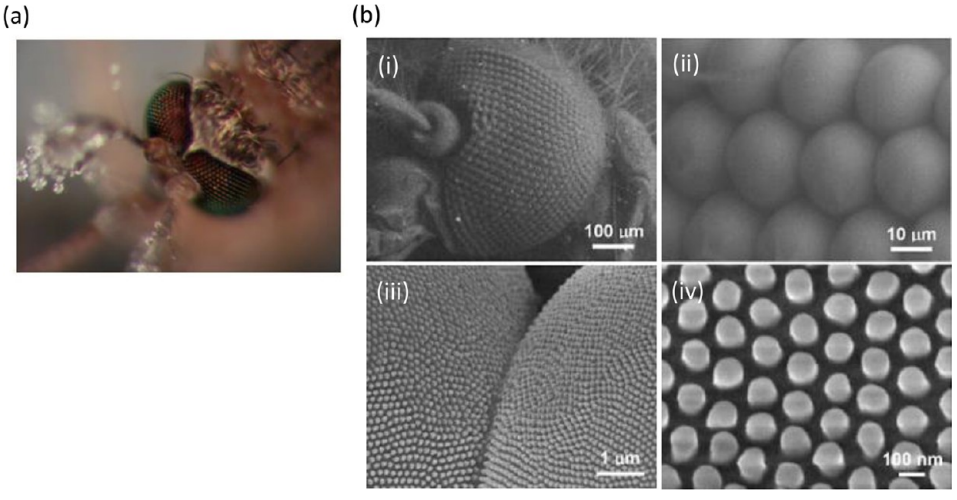

Figure 9. (a) Image of mosquito eyes, which are antifogging. (b) SEM images of (i) mosquito eye, (ii) hcp microhemispheres (ommatidia) on the surface of the eye, (iii) ommatidia, and (iv) microstructure that covers the ommatidial surface.[203] Reproduced with permission from ref 203. Copyright 2007 John Wiley and Sons.

and solid states, as shown in Figure 7.[195] The transparency of the nanoenoki PET did not change after staining as the nanoenoki structure repels the dried liquid and keeps the surface clean (Figure 7a). Optical images of wet and dried stains of mustard and blood are shown in Figure 7b(i,ii), respectively. Stains on bare PET are also shown in this figure for comparison. The adhesion forces of the dried liquids are small so that the liquid rolls away easily with slight tilting and the dried liquid easily flakes off the surface, as shown in Figure 7c.

https://dx.doi.org/10.1021/acsnano.0c06452
ACS Nano XXXX, XXX, XXX−XXX

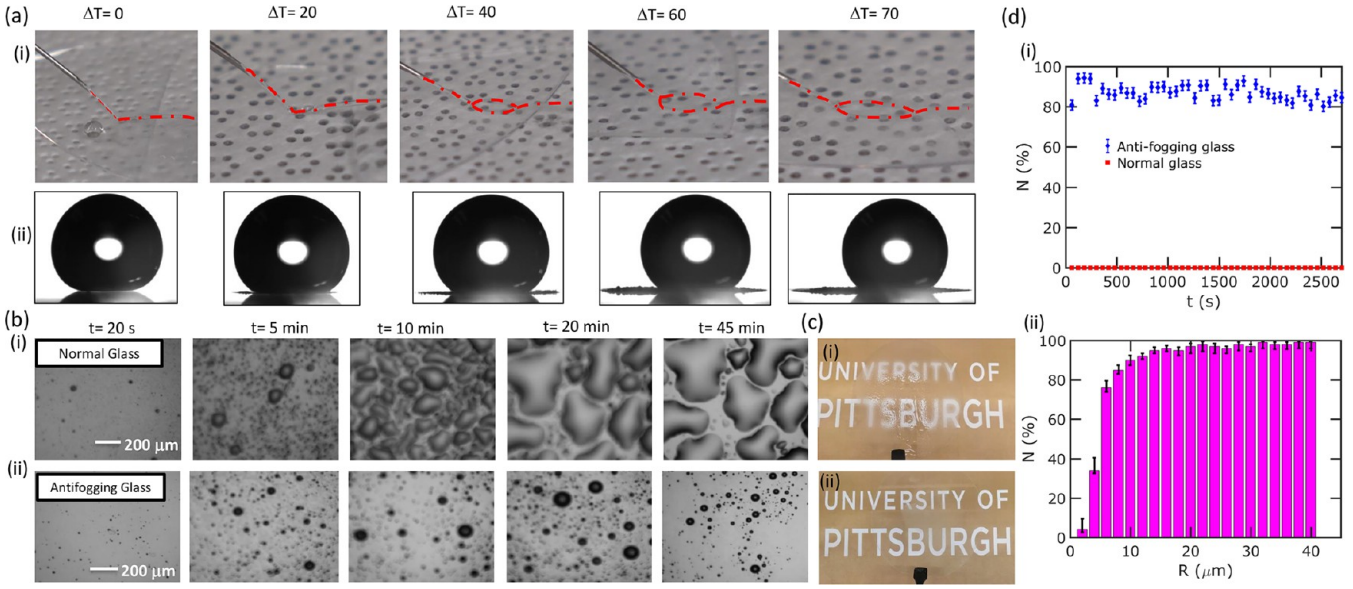

Figure 10. (a) (i) Optical images of water jet with various temperatures hitting antifogging glass. ΔT is the difference in temperature between the water and the surface. (a) (ii) Microscopic images of water droplets on the antifogging glass surface with different ΔT. (b) Optical microscope images of condensation on (i) bare and (ii) antifogging glass over time period of 45 min. The optical images after condensation are shown in (c) for (i) bare and (ii) antifogging glass. (d) (i) Plot of the percent of droplets that jump away from the substrate over time for both bare and antifogging glass. (d) (ii) Plot of the percent of jumping water droplets versus radius of the coalescent droplets.[2] Reproduced with permission from ref 2. Copyright 2019 The Royal Society of Chemistry.

Antifogging. Condensation-resistant substrates are important for antifogging applications.[2,145,146] Re-entrant structures can repel different liquids, but tiny droplets may penetrate inside the structure. During condensation, droplets can nucleate in the microstructures and propagate, pushing out the trapped air, which results in a transition from a Cassie–Baxter to a Wenzel wetting state.[184,197−201] Hot liquids may also cause failure when in contact with re-entrant structured surfaces by nucleation and growth of droplets on the cooler substrate.[145,202]

Figure 8 shows how repellency can be lost due to condensation. Condensed droplets may lead to a transition from a Cassie–Baxter state to a Wenzel state (Figure 8a). Figure 8b shows environmental scanning electron microscope (ESEM) images of the condensation of droplets between pillars. Figure 8c shows the transition of a droplet from a Cassie–Baxter state to a Wenzel state when the substrate is wicking. After droplets nucleate, the droplets grow because of the wicking substrate and fill all the empty spaces between the pillars and repellency is lost. Figure 8d shows optical images of the same substrate where repellency has been lost due to this process. Nonwicking re-entrant cavities prevent growing of the water nucleates as shown in Figure 8e.[146] The nanoscale structures are smaller than nucleation droplets and therefore prevent nucleation. However, the silicon used in this work is nontransparent at wavelengths smaller than the mid-infrared. It remains to be seen if these principles may be adapted for transparent optical materials without affecting the optical properties.

Surfaces found in nature such as mosquito compound eyes,[203] superhydrophobic cicada wings,[204] and glasswing butterfly wings[2] offer practical ways to avoid condensation and retain repellency even in humid environments through feature sizes smaller than mist droplets. Figure 9a shows an optical image of mosquito eyes resisting condensing water droplets. Figure 9b(i–iv) shows SEM images at different length scale features of a single mosquito eye. The eye consists of packed microhemispheres about 30 μm in diameter. The microhemispheres are textured with nanoscale nipples approximately 100 nm in diameter that are hexagonally packed 20 nm apart. The antifogging properties are influenced by the multilength scale structuring of the moth eyes.

There are two main approaches to achieve antifogging: (a) wet-style and (b) dry-style. The wet-style approach relies on superhydrophilicity. Photocatalytic TiO_2 nanoparticle coatings have been demonstrated to become superhydrophilic under UV irradiation.[147,205−209] In this approach, micrometer-sized water droplets spread easily and quickly and make a thin film that covers the surface and helps to reduce reflection and light scattering from tiny water islands. Dry-style is preferred to wet-style particularly in optoelectronic applications such as displays or applications like glasses and sunglasses where wetting the screen, TV, or glass is not an option. Gao *et al.* reported a superhydrophobic approach[203] and used soft lithography technique to fabricate nanoscale closed-packed nipples similar to those in mosquito eyes (Figure 9a). Although there are some reports on superhydrophobic, antifogging nontransparent substrates,[210] the number of reported articles on transparent, superhydrophobic antifogging substrates are limited.

Recently, we reported on high transparency glass based on the glasswing butterfly structure with more than 90% antifogging efficiency.[2] We measured the antifogging behavior of the fabricated nanostructures by dispensing water droplets with a significant difference in temperature with the glass substrate on the surface as well as exposing the glass substrate to a humid environment with controlled humidity over a specific time period. As shown in Figure 10a, when hotter water jets touch the cold substrate, larger wetting areas are formed caused by the significant nucleation of small droplets (Figure 10a(ii)). However, the antifogging glass shows

https://dx.doi.org/10.1021/acsnano.0c06452
ACS Nano XXXX, XXX, XXX−XXX

incredible hot water repellency. The small water nuclei move quickly and roll away off the substrate.

The glass samples were placed in a high humidity environment (about 80% humidity) to facilitate the formation of condenstaion on the surface. Figure 10b shows the nucleation and growth of water droplets on (i) bare and (ii) normal glass over time. For the normal glass, the small water nuclei grow and merge together and ultimately cover the whole surface. As a result, the transparency of the glass reduced significantly after 45 min, as shown in Figure 10c(i). However, on the antifogging glass, water nuclei roll away from the surface when they reach a specific size and after 45 min, the surface remains transparent and clean, as shown in Figure 10c(ii). We also quantified the antifogging efficiency as defined by the number of droplets that roll away and jump off the glass substrate over the total droplets formed on the glass (N),[145] over time, as shown in Figure 10d(i) for both bare and antifogging glass. More than 90% of the droplets that form on the antifogging glass jump off shortly after formation; however, nearly no droplets jump off the normal glass. In addition, Figure 10d(ii) shows the size dependency of the jumping droplets. The droplets start to jump off the glass when their size reaches around 2 μm and almost all ($N \approx 99\%$) of the droplets with size of 12 μm and above jump off the antifogging glass substrate.

Anti-icing. Icing may cause damage to optoelectronics such as solar panels, displays, sensors, or other outdoor applications. Currently, antifreeze fluids and heating the substrates are the most common strategies employed to combat icing. Surface engineering has recently been used to reduce ice formation and the adhesion of ice to the surface. Anti-icing depends on superhydrophobicity as well as the length scales of the features of the surface.[211] Classical heterogeneous nucleation theory suggests that smaller features increase the energy barrier for ice formation.[212] The lack of commercially viable fabrication processes might be an obstacle for spreading anti-icing technologies based on superhydrophobic surfaces with small feature sizes.[213]

Recently, various lubricants have been infused into porous superhydrophobic surfaces to make the substrate slippery.[214] On these slippery substrates, cold water droplets rolled away off the surfaces. Also, phase change liquids (PCL) have been shown to delay frost formation by releasing latent heat as water droplets condense on the substrate. PCL have a melting point higher than the freezing point of water and remain in a liquid state under ambient conditions.[215] Solidified PCL surfaces display varying degrees of optical transparency and can repel various types of liquids.[215] However, using a lubricating technique, such as porous surfaces or PCL, may not be a viable option for optoelectronics due to the requirement of a top liquid layer, which is not preferable for substrates that are adjacent to electronic circuits.

The fabrication of superhydrophobic substrates with ultralow hysteresis, high condensation resistance, and good mechanical durability are needed for optoelectronic substrates. Stainless steel surfaces have been fabricated with superhydrophobicity, anti-icing properties, and mechanical durability. However, these surfaces are not optically transparent.[216] There is a need to research this functionality more with regard to transparent materials.

DURABILITY OF OPTOELECTRONIC DEVICES

Optoelectronic substrates and barrier layers are important protective layers in the encapsulation of optoelectronic devices where they play an effective role in determining the long-term durability of the optoelectronic device. The substrate/barrier layer must restrict the diffusion of oxygen and water vapor which may interact with and degrade various optoelectronic components. The substrate also acts as an important protective layer for the optoelectronic device, which may degrade under the influence of many external stressors, such as high temperatures or moisture. Different approaches can be used to enhance the durability and stability of multifunctional optoelectronic substrates.

Glass offers the best barrier properties; therefore, most device applications utilize glass as a substrate or top sheet. Glass cover sheets sealed with epoxy resin[217−219] are used in solar modules, displays, and sensors. Desiccants included within an air gap are utilized for OLED technology.[220] Glass is a thicker, crystalline solid compared to thinner, semicrystalline polymers or paper, which have cavities that promote vapor species permeation. Different optical properties have been investigated for glass and various PET substrates as barrier films.[221] Polymers and paper offer higher film flexibility; however, their barrier properties need improvement for optoelectronic devices. There is great interest in a variety of different barrier/encapsulation strategies to improve the lifetime of devices including atomic layer deposition on glass[222] and polymers,[223] polymer nanocomposite films,[224] and fibrillar cellulose films.[19,21,116]

In addition to barrier properties, the various properties and functionalities of the optoelectronic device must be maintained in the presence of various stressors. For example, while a variety of photon management properties and functionalities have been demonstrated in optoelectronic substrates and barrier layers, mechanical durability of many of these surfaces are still an important issue. Even with finger touching or cleaning with soft tissues, many of these functionalities on optoelectronic substrates can be damaged.[225−230] Failure may occur in the structure itself (topography) or in the chemical coating or in both. The most common durability characterization techniques have been extensively reviewed before.[196,226,228] In particular, Bayer recently reviewed challenges and advances in the durability of transparent water repellent coatings and future research directions and considerations for transparent superhydrophobic coatings that resist wear.[196]

Methods to characterize the mechanical durability of these substrates include linear/rotary wear abrasion, tape peeling, pencil tests, macro/micro scratching, liquid impalement, and powder/spray exposure. ASTM standards from the paint industry provides standard mechanical durability testing methods. Different types of abradant and downward pressure may be applied in these different tests. Resistance to standard wear abrasion is the primary indicator of mechanical durability; however, secondary testing such as resistance to tape peeling, blade scratching, powder/spray exposure, elevated temperatures, UV light exposure, and solvent resistance may be conducted and reported.

In this section, we will review the most successful and recent durable transparent substrates and barrier layers by focusing on (1) optoelectronic device stability to vapor species, environmental stressors, and liquid droplets, (2) substrate or barrier

https://dx.doi.org/10.1021/acsnano.0c06452
ACS Nano XXXX, XXX, XXX−XXX

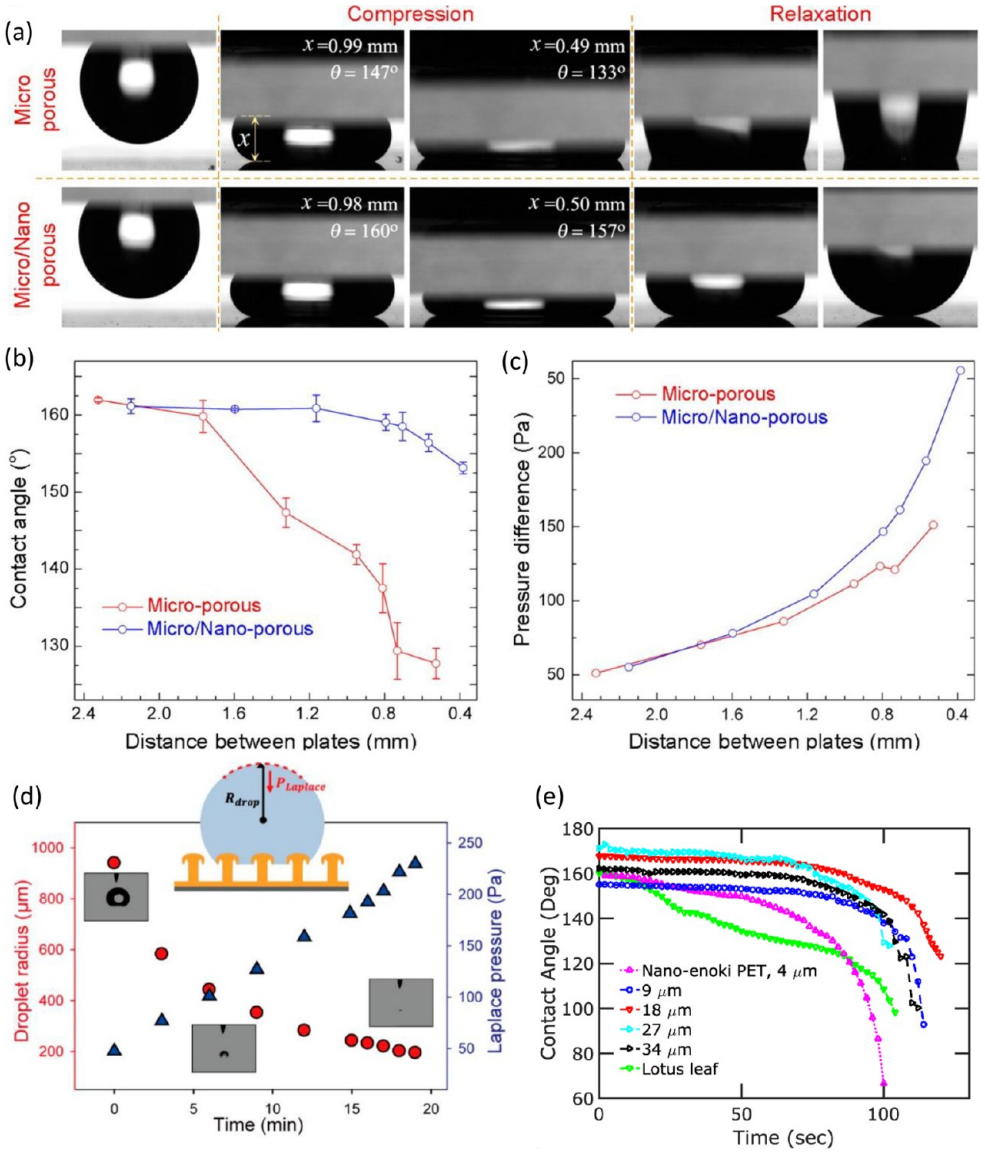

Figure 11. (a) Optical images of water droplet pressurized tests on micro and nano/microporous structures. (b,c) Plots of the contact angle and pressure difference as a function of distance between plates for microporous and micro/nanoporous structures, respectively.[248] (d) Relationship between droplet radius and laplace pressure as a function of time.[183] (e) Static contact angle *versus* time plot for nanoenoki mushroom-like PET with various pillar heights of 4, 9, 18, 27, and 34 μm compared to the lotus leaf.[195] (a), (b), and (c) reprinted from ref 248. Copyright 2014 American Chemical Society. (d) reprinted from ref 183. Copyright 2017 American Chemical Society. (e) Reproduced with permission from ref 195. Copyright 2019 The Royal Society of Chemistry.

layer property and functionality durability, and (3) durability strategies.

Device Stability. Optoelectronic devices require barrier/encapsulation properties, or specifically water and oxygen vapor hermeticity. OLEDs and organic devices are sensitive to degradation by diffusion of vapor species. Vapor permeation is also a major issue for perovskites, which are among the most moisture-sensitive optoelectronics applications.[231] Organic layers will react with molecular oxygen and water to cause degradation. In general, vapor species such as water and oxygen pass through sub-nanometer pinholes and diffuse into the cathode, producing hydrogen gas by reacting with the cathode. The performance and lifetime of the device degrades as vapor species permeate. Therefore, optoelectronic devices require encapsulation strategies with extremely low water vapor and oxygen permeability to ensure adequate lifetime.

A common device requirement for optoelectronics is a low water vapor transmission rate (WVTR).[232] WVTR is a measure of the passage of water vapor through a substance. Standard methods such as ASTM or ISO are utilized when measuring WVTR levels where temperature and humidity must be controlled and reported. Commercially available films used to protect OLEDs have a WVTR of about 10^{-3}–10^{-6} g m^{-2} per day at 25 °C and 90% relative humidity. Recent research focuses on reducing the WVTR of the substrate without altering the substrate optical properties for optoelectronic device stability.

Glass substrates are widely used for encapsulations and considered the norm for evaluating alternative encapsulation methods.[223,233] The reduction of glass thickness and fabrication of flexible glass preserves the barrier properties of the glass since the fabrication process of normal and flexible

https://dx.doi.org/10.1021/acsnano.0c06452
ACS Nano XXXX, XXX, XXX−XXX

glass is similar and both of them are made of molten glass that prevents the formation of pinhole defects.[16] Although adhesives and glass frit bonding can be used for sealing the glass in the encapsulation process, there are still limitations in hermetically encapsulating devices using normal and flexible glass, such as edge sealing.[16]

Multiple layers of barrier films can be deposited to enhance the barrier properties of polymer films. The chance of existing pinhole defects in these types of structures is high. Encapsulation techniques by thin film layering using atomic layer deposition (ALD) have been reported to reduce pinhole defects for improved barrier properties. Single Al_2O_3 ALD films on polymers showed WVTR as low as 10^{-3} g m^{-2} per day, whereas two bilayers of Al_2O_3 and SiO_2 reduced the effective WVTR to $\approx 5 \times 10^{-5}$ g m^{-2} per day.[234] Additionally, alternating thin film layers of Al_2O_3 by ALD and parylene by chemical vapor deposition showed enhanced barrier properties for OLEDs.[235] The multilayer ceramic−polymer thin film obtained a WVTR value lower than 10^{-5} g m^{-2} per day. Polymer nanocomposites such as polyimide/graphene oxide[224] have also been used to enhance barrier properties from vapor species.

Paper substrates typically perform poorly when it comes to moisture protection. This is one of the main challenges that limits the application of paper substrates in optoelectronics. Strategies to improve moisture protection for paper substrates include oxidized cellulose,[21] carboxymethylated microfibril cellulose,[116] nanostructured wood fibers,[37] and nanofibril cellulose.[19] Future improvements in barrier properties for optical device stability are highly desirable.

Stability to Stressors. There are a range of external stressors that can hinder the performance of optoelectronic substrates or barrier films such as exposure to high temperature, salt water, and UV. The multifunctionality of the optoelectronic substrate must be durable enough to withstand different environments. There are protocols for assessing the durability of superhydrophobic surfaces after exposure to various stressors;[236] however, there are no standards or protocols to test the durability of multifunctional optoelectronic substrates or barrier films. Typically, the multifunctionality is tested after exposure to stressors such as heat, light, various solvents, and liquid impalement.

Numerous coating strategies have been tested for improving the durability of multifunctional surfaces against external stressors. A transparent superhydrophobic gel showed superhydrophobicity up to 6 h at 150 °C and self-healing up to eight cycles after being damaged by 1 M HCl.[237] A transparent superhydrophobic surface from porous silica capsules maintained properties at 400 °C for 10 h.[238] A durable, sprayable polyurethane−acrylic colloidal suspension was shown to preserve 70% transparency at 400 nm and superhydrophobic performance after 50 h exposure to strong UVC light (254 nm, 3.3 mW/cm^2), 24 h of oil contamination, and 24 h of highly acidic conditions (1 M HCl).[239] Long-term durability of transparent, superhydrophobic silicone nanofilament coatings has been shown by outdoor weathering for 12 months, acid dew and fog tests, and 240 h of UV-lamp exposure.[240] Mesh structure enhanced superhydrophobic surfaces maintained superhydrophobicity and transparency of about 80% after 240 min of exposure to liquids with a pH range of 2−14.[241] Armored PDMS films by laser ablation have maintained superhydrophobicity and transparency of about 90% after 8 times the density of sunlight exposure or at elevated temperatures of 325 °C.[242] Future work should improve on the performance of optoelectronic substrates against various external stressors and work toward standardized testing protocols.

Stability to Liquid Droplets. In this section, we focus on one method to characterize durability using the pressure stability of liquid droplets. Cassie−Baxter state stability has been investigated in several works,[167,243−245] where the thermodynamic stability of the droplet and structure was thoroughly studied.

Various research groups have used pressure tests to examine the thermodynamic stability of the observed Cassie−Baxter state.[246−248] For instance, surface topography effects on Cassie−Baxter state stability were studied on superhydrophobic glass.[248] Glass substrates were coated with different combinations of micro/nanoporous layers, and the pressurized droplet test was used to study Cassie−Baxter state stability. Figure 11a shows the comparison test of a water droplet between a nanoporous hydrophobic coating plate at the bottom and a microporous superhydrophobic coating at top. For the microporous structure, after compression and in relaxation mode, water droplets stick to the surface which indicates a transition to a Wenzel state; however, for micro/nanoporous structure in relaxation mode, water droplets do not stick to plates and stay in a Cassie−Baxter state. To quantify the stability of the Cassie state, *in situ* contact angle and pressure as a function of distance between plates measurements have been reported, as shown in Figure 11b,c, respectively. The transition to Wenzel state happened at 80 Pa for the microporous structure, whereas micro/nanoporous structures could tolerate high pressure of 260 Pa.

In addition to pressurized water droplets, slow evaporation of sitting droplets on the surface while monitoring changes in contact angle, is another common method to evaluate the stability of Cassie−Baxter state.[183,195,248] Figure 11d shows the relationship between evaporating ethanol droplet radius dispensed on mushroom-like pillars and Laplace pressure calculated from

$$P(t) = 2\gamma_{LV}/R(t) \tag{9}$$

where γ_{LV} is ethanol surface energy.[183] By evaporating the droplet, its radius becomes smaller, which increases the Laplace pressure inside the droplet. When the radius of the droplet was about 195 μm, the contact angle dropped suddenly, which indicates that the droplet transitioned to a Wenzel state from a Cassie−Baxter state. The equivalent Laplace pressure corresponding to this radius is 230 Pa, which is considered its breakthrough pressure. The breakthrough pressure is defined as the pressure at the sudden drop in contact angle point where the droplet penetrates inside the structure and a transition from Cassie−Baxter to Wenzel state happens.[243]

We also used evaporating droplet experiments to measure the stability of the Cassie−Baxter on nanoenoki mushroom-like structures on PET.[195] Figure 11e shows the change in contact angle of a single water droplet sitting on the nanoenoki PET with different pillar heights over time. A sudden drop in contact angle is an indication of the droplet breaking through into the nanostructure and transitioning to a Wenzel state. As can be seen in Figure 11e, a sudden drop in contact angle was observed in 4 μm tall nanonenoki. This experiment shows that taller nanoenoki mushroom structures prevent the droplet from breaking through and touching the substrate.[249]

https://dx.doi.org/10.1021/acsnano.0c06452
ACS Nano XXXX, XXX, XXX−XXX

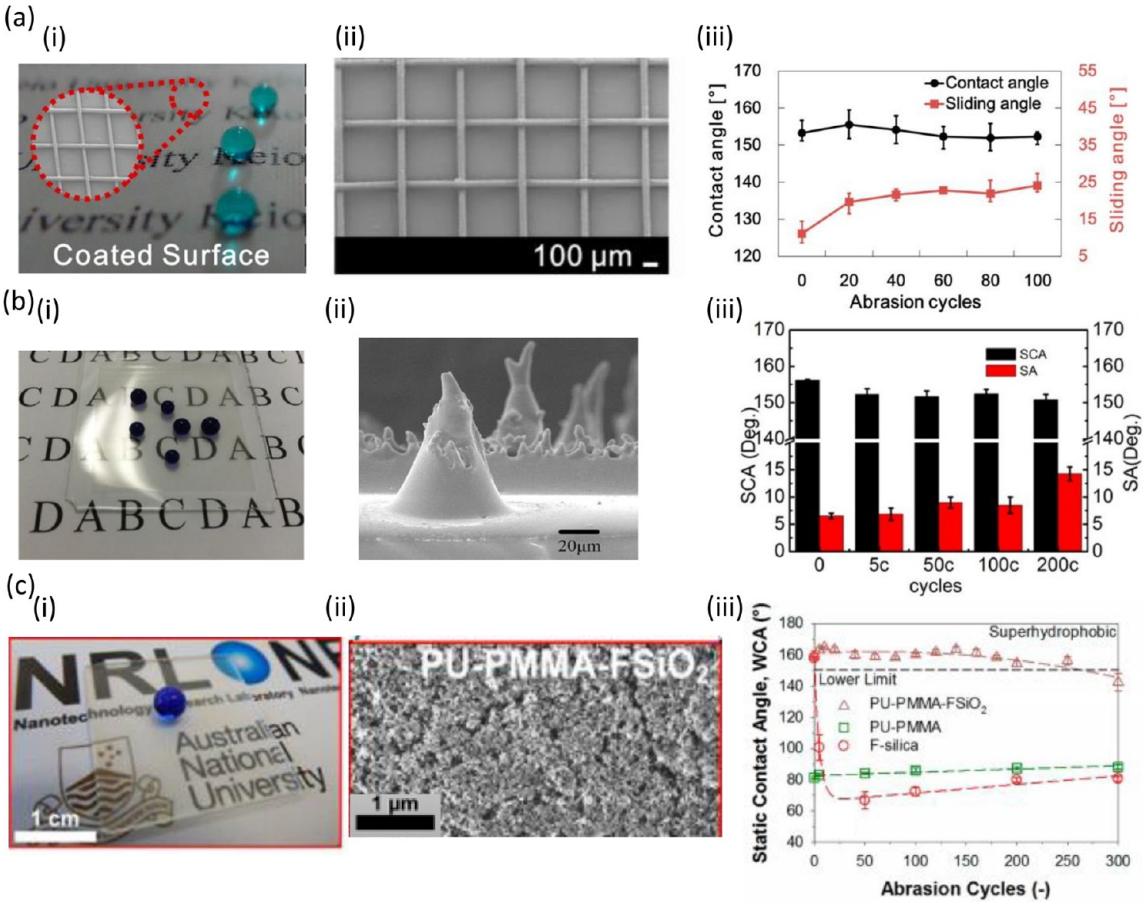

Figure 12. (i) Optical image, (ii) SEM image, and (iii) abrasion cycle plot for (a) superhydrophobic polyester mesh,[241] (b) transparent PDMS surface with superhydrophobicity,[242] and (c) self-assembly hierarchical interpenetrated polymer networks.[239] (a) Reprinted from ref 241. Copyright 2015 American Chemical Society. (b) Reprinted from ref 242. Copyright 2016 American Chemical Society. (c) Reprinted from ref 239. Copyright 2016 American Chemical Society.

We observed a droplet with radius of about 160 μm without any breakthrough. This radius corresponds to more than 900 Pa in Laplace pressure. Most research on re-entrant structures such as micropillar mushroom-like arrays[183] or hierarchical structures[167] exhibit lower breakthrough pressures. The pitch size, or the distance between adjacent pillars, in those studies is more than 20 μm. However, nanoenoki PET are approximately 5 μm apart, which provides a significant energy barrier for infiltration. Fabrication of re-entrant structures with smaller pitch size can significantly enhance the breakthrough pressure and needs to be studied more in the future.

Substrate Property and Functionality Durability. This section focuses on current fabrication and characterization strategies for mechanical abrasion durability for optoelectronic substrates. While there have been multiple efforts to produce mechanically durable transparent superhydro/oleophobic coatings,[149,237,238,250−262] the number of successful research reports with very high transparency (>90%) and mechanical robustness is very limited. Adhesion or welding of transparent primers or nanoparticles on top of transparent flexible plastic surfaces by methods such as thermal annealing as well as self-similar layering have been recently reported.[196] A variety of abrasion resistance testing against wear, scratching, peeling, and/or powder/spray exposure is a very important aspect that is missing in much research. Some works have used the tape peel test or sand grain test as an alternative to an abrasion test.[238] However, durability against mechanical abrasion determines the capabilities of the coating to be used in real life applications.

Figure 12a(i) shows an optical image of a mechanically durable polyester mesh that demonstrated both superhydrophobicty as well as high transparency.[241] This structure was fabricated using low surface tension coated fibers, coated with low surface energy SiO_2 nanoparticles. An SEM image of this mesh-like structure is shown in Figure 12a(ii). After 100 abrasion cycles at a pressure of 10 kPa (with cotton textile), this structure showed water contact angle of more than 150° with sliding angle less than 25°, as well as transmission of 79%. However, a transparency of less than 80% after abrasion tends to be lower than what is needed for optoelectronics.

Figure 12b(i) shows transparent PDMS with superhydrophobicity.[242] The microstructure on the PDMS is shown in Figure 12b(i). These structures consisted of microgrooves and microhole arrays duplicated by using a laser-ablated template. The water contact angle and sliding angles were reported as 154.5 ± 1.7 and 6 ± 1.7°, respectively, initially, and that there were only slight changes after 100 cycle of abrasion under 300 gr load with sand paper, as shown in Figure 12b(i).

Figure 12c shows (i) optical and (ii) SEM images of a transparent polymer made of self-assembled hierarchical interpenetrated polymer networks.[239] This structure showed abrasion resistance by maintaining superhydrophobicity after 120 abrasion cycles under a 250 g load based on ASTM D4060

https://dx.doi.org/10.1021/acsnano.0c06452
ACS Nano XXXX, XXX, XXX−XXX

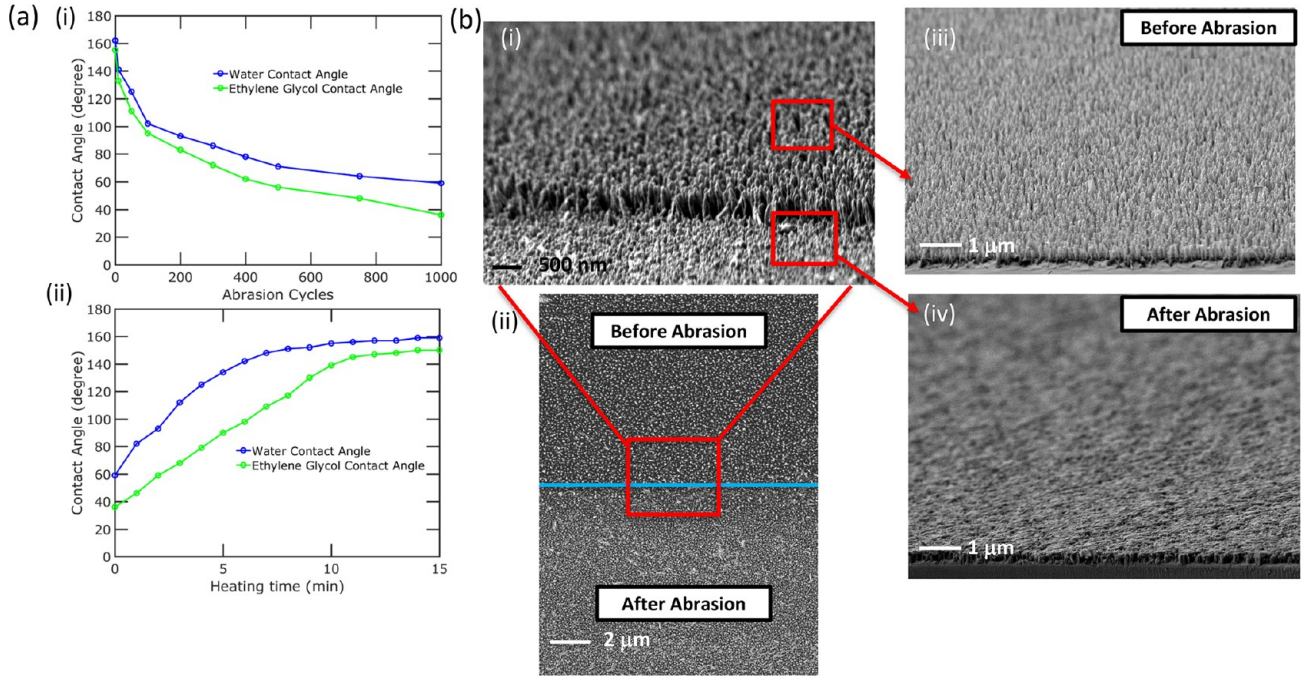

Figure 13. (a) (i) Static contact angle of water and ethylene glycol droplets as a function of abrasion cycles. (ii) Increasing static water and contact angle of water and ethylene glycol droplets as a function of heating time. (b) (i) Cross section and (ii) overhead SEM images of nonabraded and abraded nanostructures after 500 abrasion cycles. (iii) Outset of nonabraded SEM images highlighting structural uniformity. (iv) Outset of abraded SEM image after 500 abrasion cycles. Reproduced with permission from ref 2. Copyright 2019 The Royal Society of Chemistry.

abrasion standards (Figure 12c(iii)). However, the transparency of the coated substrate is about 70% at 400 nm wavelength, which may not be high enough for optoelectronic applications, where over 90% is generally desired.

Durability Strategies. Several strategies can be used to fabricate a mechanically durable functional coating: (a) constraining material elimination to keep performance under abrasion, (b) designing self-similar materials, and (c) introducing self-healing properties where the surface can retain its initial characteristics after healing. Verho *et al.*[263] reviewed several methods for mechanically durable superhydrophobic surfaces including self-similar layering and self-healing. In self-similar layers, as the coating wears away, the newly exposed layers are self-similar and thus, maintain the properties of the previously exposed top layer. In self-healing surfaces, the coating regenerates its original texture with hydrophobic chemistry by the aid of external stimulus. However, durable transparent substrates have not been reviewed. There exist some reports on nontransparent, durable, nonwetting coatings based on polymer nanocomposites;[128,226] however, these strategies are not viable for optoelectronic substrates or barrier films. There are few reports of mechanically durable, nonwetting coatings for optoelectronic applications.

Self-similar layers of low surface energy material is a strategy to maintain durable, nonwetting performance.[128] Glass slides have been coated by silicone nanofilaments with antireflective, transparent properties to test the long-term environmental durability.[240] Static and sliding water contact angles were characterized for over 30 days; the transmittance was up to 93% after 12 months of outdoor exposure to UV light and rainfall. Aytug *et al.* fabricated nanoscale pores surrounded by silica nanostructure on glass which showed antireflective properties as well as abrasion resistance.[264] Nanoindentation and drop tests of 50 g of Al_2O_3 were used to demonstrate the antiscratch properties of the films by self-similar layering; however, the abrasion resistance by mechanical abrasion of the film was not reported. These abrasion resistant transparent coatings can be a good candidate to be used for antigraffiti applications.

Another strategy for the fabrication of robust coatings is the use of self-healing materials. This class of materials have the capability of repairing damage that might have been created with external forces such as dust, heat, and friction. Polymeric self-healing materials have been investigated broadly.[265−270] Similarly, self-healing fabric materials have been reported in several works.[166,271] However, these substrates have not been suitable for optoelectronics because they are not sufficiently transparent. There is a lack of research in durability strategies (such as self-similarity or self-healing) that are specifically for optoelectronic substrates or barrier films that maintain functionality and optical properties.

Recently, we reported the fabrication of self-healing, superomniphobic transparent glass.[2] The random nanostructure of our superomniphobic glass, provides for self-similarity as well as self-healing ability. We used a Scotch-Brite abrasive pad with a pressure of 1225 N/m^2 for abrading the nanostructure. The water and oil contact angle after 400 cycles of abrasion reduced significantly as shown in Figure 13a(i). However, after heating the glass substrate at 95 °C for 15 min, the water and oil contact angle increased to near initial values, as shown in Figure 13a(ii). The main reason for this self-healing behavior comes from two characteristics of the surfaces: the abraded structures are very similar to the nonabraded structures, and flourine molecules are mobile, so with heating they find their path to the surface and help to

https://dx.doi.org/10.1021/acsnano.0c06452
ACS Nano XXXX, XXX, XXX−XXX

reduce the surface energy, similar to epicuticular wax in plant cuticles.[272]

The nanostructure of our superomniphobic glass is shown in Figure 13b(i–iv), before and after abrasion, respectively, with different magnifications. After the abrasion for 500 cycles, the height of the pillars decreased; however, the re-entrant shape of the structure did not change significantly in comparison with nonabraded samples.

Self-similar structures as well as low surface tension molecules trapped in the structure are keys to retaining the superomniphobic properties. However, there are still several limitations in this approach as, ultimately after several thousand of abrasion cycles or much higher load, all the surface structures would be destroyed. This field needs much more research particularly for glass and paper substrates. For future research, the fabrication of a self-healing structure that does not use low surface tension materials or are able to self-roughen without sacrificing optical properties could lead to a revolution in optoelectronic substrates.

CONCLUSION

Research on optoelectronic substrates will promote the development of various applications in industries from energy to electronics. Advancements in optoelectronic substrates and barrier layers have been inspired by nature and offer a wide variety of functionalities that improve technological performance. These functionalities include antireflection, light absorption, haze control, liquid repellency, antisoiling, self-cleaning, stain resistance, antifogging, and anti-icing. A range of advances and future prospects in optoelectronic substrate research have been summarized and discussed. Techniques to characterize and compare liquid droplet stability were introduced. Functionality durability strategies such as reducing wear removal, self-similar layering and self-healing were compared. Efficiency, protection from the ambient environment, and durability remain key challenges for optotoelectronic substrates and barrier layers. Future research will impact the development of solar module technology, lighting, displays, wearables, sensors, and more.

AUTHOR INFORMATION

Corresponding Author

Paul W. Leu − *Department of Industrial Engineering, Department of Mechanical Engineering, and Department of Chemical Engineering, University of Pittsburgh, Pittsburgh, Pennsylvania 15261, United States*; Email: pleu@pitt.edu

Authors

Sajad Haghanifar − *Department of Industrial Engineering, University of Pittsburgh, Pittsburgh, Pennsylvania 15261, United States*; orcid.org/0000-0003-2620-4792

Anthony J. Galante − *Department of Industrial Engineering, University of Pittsburgh, Pittsburgh, Pennsylvania 15261, United States*; orcid.org/0000-0002-1227-6771

Complete contact information is available at: https://pubs.acs.org/10.1021/acsnano.0c06452

Notes

The authors declare no competing financial interest.

ACKNOWLEDGMENTS

This work was supported in part by the National Science Foundation (ECCS 1552712).

VOCABULARY

Optoelectronic, electronic devices that use light, such as light emitting diodes(LED's) and solar cells

Bio-inspired, inspired by biological structures, features and models

Superhydrophobic, surfaces that demonstrate static contact angles more than 150° and hysteresis less than 10° for water

Superomniphobic, surfaces that demonstrate static contact angles more than 150° and hysteresis less than 10° for all types of liquids

Antireflection coating, type of an optical coating used in industry to reduce reflection of an optical device

Broadband antireflection, property of a surface with reduced reflection across a broad range of wavelengths

Omnidirectional antireflection, property of surface with reduce reflection across all possible incidence angles

REFERENCES

(1) Haghanifar, S.; Lu, P.; Kayes, M. I.; Tan, S.; Kim, K.-J.; Gao, T.; Ohodnicki, P.; Leu, P. W. Self-Cleaning, High Transmission, Near Unity Haze OTS/Silica Nanostructured Glass. *J. Mater. Chem. C* **2018**, *6*, 9191–9199.

(2) Haghanifar, S.; McCourt, M.; Cheng, B.; Wuenschell, J.; Ohodnicki, P.; Leu, P. W. Creating Glasswing Butterfly-Inspired Durable Antifogging Superomniphobic Supertransmissive, Superclear Nanostructured Glass through Bayesian Learning and Optimization. *Mater. Horiz.* **2019**, *6*, 1632–1642.

(3) Wong, T.-S.; Kang, S. H.; Tang, S. K. Y.; Smythe, E. J.; Hatton, B. D.; Grinthal, A.; Aizenberg, J. Bioinspired Self-Repairing Slippery Surfaces with Pressure-Stable Omniphobicity. *Nature* **2011**, *477*, 443–447.

(4) Raut, H. K.; Ganesh, V. A.; Nair, A. S.; Ramakrishna, S. Anti-Reflective Coatings: a Critical, In-Depth Review. *Energy Environ. Sci.* **2011**, *4*, 3779–3804.

(5) Chen, Y.-C.; Huang, Z.-S.; Yang, H. Cicada-Wing-Inspired Self-Cleaning Antireflection Coatings on Polymer Substrates. *ACS Appl. Mater. Interfaces* **2015**, *7*, 25495–25505.

(6) Siddique, R. H.; Gomard, G.; Hölscher, H. The Role of Random Nanostructures for the Omnidirectional Anti-Reflection Properties of the Glasswing Butterfly. *Nat. Commun.* **2015**, *6*, 6909.

(7) Haghanifar, S.; Rodriguez De Vecchis, R. T; Kim, K.-J.; Wuenschell, J.; Sharma, S. P; Lu, P.; Ohodnicki, P.; Leu, P. W Flexible Nanograss with Highest Combination of Transparency and Haze for Optoelectronic Plastic Substrates. *Nanotechnology* **2018**, *29*, 42LT01.

(8) Haghanifar, S.; Gao, T.; Rodriguez De Vecchis, R. T.; Pafchek, B.; Jacobs, T. D. B.; Leu, P. W. Ultrahigh-Transparency, Ultrahigh-Haze Nanograss Glass with Fluid-Induced Switchable Haze. *Optica* **2017**, *4*, 1522–1525.

(9) Park, K.-C.; Choi, H. J.; Chang, C.-H.; Cohen, R. E.; McKinley, G. H.; Barbastathis, G. Nanotextured Silica Surfaces with Robust Superhydrophobicity and Omnidirectional Broadband Supertransmissivity. *ACS Nano* **2012**, *6*, 3789–3799.

(10) Müller-Meskamp, L.; Kim, Y. H.; Roch, T.; Hofmann, S.; Scholz, R.; Eckardt, S.; Leo, K.; Lasagni, A. F. Efficiency Enhancement of Organic Solar Cells by Fabricating Periodic Surface Textures Using Direct Laser Interference Patterning. *Adv. Mater.* **2012**, *24*, 906–910.

(11) Han, T.-H.; Lee, Y.; Choi, M.-R.; Woo, S.-H.; Bae, S.-H.; Hong, B. H.; Ahn, J.-H.; Lee, T.-W. Extremely Efficient Flexible Organic Light-Emitting Diodes with Modified Graphene Anode. *Nat. Photonics* **2012**, *6*, 105–110.

https://dx.doi.org/10.1021/acsnano.0c06452
ACS Nano XXXX, XXX, XXX–XXX

(12) Zhou, L.; Wanga, A.; Wu, S.-C.; Sun, J.; Park, S.; Jackson, T. N. All-Organic Active Matrix Flexible Display. *Appl. Phys. Lett.* **2006**, *88*, 083502.
(13) Gelinck, G. H.; Huitema, H. E. A.; van Veenendaal, E.; Cantatore, E.; Schrijnemakers, L.; van der Putten, J. B. P. H.; Geuns, T. C. T.; Beenhakkers, M.; Giesbers, J. B.; Huisman, B.-H.; Meijer, E. J.; Benito, E. M.; Touwslager, F. J.; Marsman, A. W.; van Rens, B. J. E.; de Leeuw, D. M. Flexible Active-Matrix Displays and Shift Registers Based on Solution-Processed Organic Transistors. *Nat. Mater.* **2004**, *3*, 106.
(14) Hecht, D. S.; Thomas, D.; Hu, L.; Ladous, C.; Lam, T.; Park, Y.; Irvin, G.; Drzaic, P. Carbon-Nanotube Film on Plastic as Transparent Electrode for Resistive Touch Screens. *J. Soc. Inf. Disp.* **2009**, *17*, 941−946.
(15) MacDonald, W. A.; Looney, M. K.; MacKerron, D.; Eveson, R.; Adam, R.; Hashimoto, K.; Rakos, K. Latest Advances in Substrates for Flexible Electronics. *J. Soc. Inf. Disp.* **2007**, *15*, 1075−1083.
(16) Garner, S. M. *Flexible Glass: Enabling Thin, Lightweight, and Flexible Electronics*; John Wiley & Sons, 2017.
(17) Zhu, H.; Fang, Z.; Preston, C.; Li, Y.; Hu, L. Transparent Paper: Fabrications, Properties, and Device Applications. *Energy Environ. Sci.* **2014**, *7*, 269−287.
(18) Ha, D.; Fang, Z.; Zhitenev, N. B. Paper in Electronic and Optoelectronic Devices. *Advanced Electronic Materials* **2018**, *4*, 1700593.
(19) Österberg, M.; Vartiainen, J.; Lucenius, J.; Hippi, U.; Seppälä, J.; Serimaa, R.; Laine, J. A Fast Method to Produce Strong NFC Films as a Platform for Barrier and Functional Materials. *ACS Appl. Mater. Interfaces* **2013**, *5*, 4640−4647.
(20) Fernandes, S. C. M.; Oliveira, L.; Freire, C. S. R.; Silvestre, A. J. D.; Neto, C. P.; Gandini, A.; Desbriéres, J. Novel Transparent Nanocomposite Films Based on Chitosan and Bacterial Cellulose. *Green Chem.* **2009**, *11*, 2023−2029.
(21) Fukuzumi, H.; Saito, T.; Iwata, T.; Kumamoto, Y.; Isogai, A. Transparent and High Gas Barrier Films of Cellulose Nanofibers Prepared by TEMPO-Mediated Oxidation. *Biomacromolecules* **2009**, *10*, 162−165.
(22) Qi, D.; Lu, N.; Xu, H.; Yang, B.; Huang, C.; Xu, M.; Gao, L.; Wang, Z.; Chi, L. Simple Approach to Wafer-Scale Self-Cleaning Antireflective Silicon Surfaces. *Langmuir* **2009**, *25*, 7769−7772.
(23) Yano, H.; Sugiyama, J.; Nakagaito, A. N.; Nogi, M.; Matsuura, T.; Hikita, M.; Handa, K. Optically Transparent Composites Reinforced with Networks of Bacterial Nanofibers. *Adv. Mater.* **2005**, *17*, 153−155.
(24) Varanasi, S.; Batchelor, W. J. Rapid Preparation of Cellulose Nanofibre Sheet. *Cellulose* **2013**, *20*, 211−215.
(25) Sehaqui, H.; Liu, A.; Zhou, Q.; Berglund, L. A. Fast Preparation Procedure for Large, Flat Cellulose and Cellulose/Inorganic Nanopaper Structures. *Biomacromolecules* **2010**, *11*, 2195−2198.
(26) Nogi, M.; Kim, C.; Sugahara, T.; Inui, T.; Takahashi, T.; Suganuma, K. High Thermal Stability of Optical Transparency in Cellulose Nanofiber Paper. *Appl. Phys. Lett.* **2013**, *102*, 181911.
(27) Yang, Q.; Fukuzumi, H.; Saito, T.; Isogai, A.; Zhang, L. Transparent Cellulose Films with High Gas Barrier Properties Fabricated from Aqueous Alkali/Urea Solutions. *Biomacromolecules* **2011**, *12*, 2766−2771.
(28) Hsieh, M.-C.; Kim, C.; Nogi, M.; Suganuma, K. Electrically Conductive Lines on Cellulose Nanopaper for Flexible Electrical Devices. *Nanoscale* **2013**, *5*, 9289−9295.
(29) Iftekhar Shams, Md.; Nogi, M.; Berglund, L. A.; Yano, H. The Transparent Crab: Preparation and Nanostructural Implications for Bioinspired Optically Transparent Nanocomposites. *Soft Matter* **2012**, *8*, 1369−1373.
(30) Nogi, M.; Yano, H. Optically Transparent Nanofiber Sheets by Deposition of Transparent Materials: A Concept for a Roll-To-Roll Processing. *Appl. Phys. Lett.* **2009**, *94*, 233117.
(31) Iwamoto, S.; Nakagaito, A.; Yano, H. Nano-Fibrillation of Pulp Fibers for the Processing of Transparent Nanocomposites. *Appl. Phys. A: Mater. Sci. Process.* **2007**, *89*, 461−466.
(32) Yang, Q.; Qin, X.; Zhang, L. Properties of Cellulose Films Prepared from NaOH/urea/zincate Aqueous Solution at Low Temperature. *Cellulose* **2011**, *18*, 681−688.
(33) Zhang, L.; Ruan, D.; Zhou, J. Structure and Properties of Regenerated Cellulose Films Prepared from Cotton Linters in NaOH/Urea Aqueous Solution. *Ind. Eng. Chem. Res.* **2001**, *40*, 5923−5928.
(34) Liu, S.; Zhang, L. Effects of Polymer Concentration and Coagulation Temperature on the Properties of Regenerated Cellulose Films Prepared from LiOH/urea Solution. *Cellulose* **2009**, *16*, 189−198.
(35) Nogi, M.; Handa, K.; Nakagaito, A. N.; Yano, H. Optically Transparent Bionanofiber Composites with Low Sensitivity to Refractive Index of the Polymer Matrix. *Appl. Phys. Lett.* **2005**, *87*, 243110.
(36) Nogi, M.; Yano, H. Transparent Nanocomposites Based on Cellulose Produced by Bacteria Offer Potential Innovation in the Electronics Device Industry. *Adv. Mater.* **2008**, *20*, 1849−1852.
(37) Fang, Z.; Zhu, H.; Yuan, Y.; Ha, D.; Zhu, S.; Preston, C.; Chen, Q.; Li, Y.; Han, X.; Lee, S.; Chen, G.; Li, T.; Munday, J.; Huang, J.; Hu, L. Novel Nanostructured Paper with Ultrahigh Transparency and Ultrahigh Haze for Solar Cells. *Nano Lett.* **2014**, *14*, 765−773.
(38) Aguas, H.; Mateus, T.; Vicente, A.; Gaspar, D.; Mendes, M. J.; Schmidt, W. A.; Pereira, L.; Fortunato, E.; Martins, R. Thin Film Silicon Photovoltaic Cells on Paper for Flexible Indoor Applications. *Adv. Funct. Mater.* **2015**, *25*, 3592−3598.
(39) Hübler, A.; Trnovec, B.; Zillger, T.; Ali, M.; Wetzold, N.; Mingebach, M.; Wagenpfahl, A.; Deibel, C.; Dyakonov, V. Printed Paper Photovoltaic Cells. *Adv. Energy Mater.* **2011**, *1*, 1018−1022.
(40) Wang, B.; Kerr, L. L. Dye Sensitized Solar Cells on Paper Substrates. *Sol. Energy Mater. Sol. Cells* **2011**, *95*, 2531−2535.
(41) Leonat, L.; White, M. S.; Głowacki, E. D.; Scharber, M. C.; Zillger, T.; Rühling, J.; Hübler, A.; Sariciftci, N. S. 4% Efficient Polymer Solar Cells on Paper Substrates. *J. Phys. Chem. C* **2014**, *118*, 16813−16817.
(42) Hu, L.; Zheng, G.; Yao, J.; Liu, N.; Weil, B.; Eskilsson, M.; Karabulut, E.; Ruan, Z.; Fan, S.; Bloking, J. T.; McGehee, M. D.; Wagberg, L.; Cui, Y. Transparent and Conductive Paper from Nanocellulose Fibers. *Energy Environ. Sci.* **2013**, *6*, 513−518.
(43) Kim, T.-S.; Na, S.-I.; Kim, S.-S.; Yu, B.-K.; Yeo, J.-S.; Kim, D.-Y. Solution-Processible Polymer Solar Cells Fabricated on a Papery Substrate. *Phys. Status Solidi RRL* **2012**, *6*, 13−15.
(44) Zhou, Y.; Fuentes-Hernandez, C.; Khan, T. M.; Liu, J.-C.; Hsu, J.; Shim, J. W.; Dindar, A.; Youngblood, J. P.; Moon, R. J.; Kippelen, B. Recyclable Organic Solar Cells on Cellulose Nanocrystal Substrates. *Sci. Rep.* **2013**, *3*, 1536.
(45) Wang, F.; Chen, Z.; Xiao, L.; Qu, B.; Gong, Q. Papery Solar Cells Based on Dielectric/metal Hybrid Transparent Cathode. *Sol. Energy Mater. Sol. Cells* **2010**, *94*, 1270−1274.
(46) Lamprecht, B.; Thünauer, R.; Ostermann, M.; Jakopic, G.; Leising, G. Organic Photodiodes on Newspaper. *Phys. Status Solidi A* **2005**, *202*, R50−R52.
(47) Ha, D.; Fang, Z.; Hu, L.; Munday, J. N. Paper-based Anti-Reflection Coatings for Photovoltaics. *Adv. Energy Mater.* **2014**, *4*, 1301804.
(48) Ha, D.; Murray, J.; Fang, Z.; Hu, L.; Munday, J. N. Advanced Broadband Antireflection Coatings Based on Cellulose Microfiber Paper. *IEEE Journal of Photovoltaics* **2015**, *5*, 577−583.
(49) Fang, Z.; Zhu, H.; Preston, C.; Han, X.; Li, Y.; Lee, S.; Chai, X.; Chen, G.; Hu, L. Highly Transparent and Writable Wood All-Cellulose Hybrid Nanostructured Paper. *J. Mater. Chem. C* **2013**, *1*, 6191−6197.
(50) Wang, X.; Gao, K.; Shao, Z.; Peng, X.; Wu, X.; Wang, F. Layer-By-layer Assembled Hybrid Multilayer Thin Film Electrodes Based on Transparent Cellulose Nanofibers Paper for Flexible Supercapacitors Applications. *J. Power Sources* **2014**, *249*, 148−155.
(51) Li, S.; Huang, D.; Zhang, B.; Xu, X.; Wang, M.; Yang, G.; Shen, Y. Flexible Supercapacitors Based on Bacterial Cellulose Paper Electrodes. *Adv. Energy Mater.* **2014**, *4*, 1301655.

https://dx.doi.org/10.1021/acsnano.0c06452
ACS Nano XXXX, XXX, XXX−XXX

(52) Razaq, A.; Nyholm, L.; Sjödin, M.; Strømme, M.; Mihranyan, A. Paper-based Energy-Storage Devices Comprising Carbon Fiber-Reinforced Polypyrrole-Cladophora Nanocellulose Composite Electrodes. *Adv. Energy Mater.* **2012**, *2*, 445−454.
(53) Preston, C.; Fang, Z.; Murray, J.; Zhu, H.; Dai, J.; Munday, J. N.; Hu, L. Silver Nanowire Transparent Conducting Paper-Based Electrode with High Optical Haze. *J. Mater. Chem. C* **2014**, *2*, 1248−1254.
(54) Peng, C. Q.; Thio, Y. S.; Gerhardt, R. A. Conductive Paper Fabricated by Layer-By-Layer Assembly of Polyelectrolytes and ITO Nanoparticles. *Nanotechnology* **2008**, *19*, 505603.
(55) Koga, H.; Nogi, M.; Komoda, N.; Nge, T. T.; Sugahara, T.; Suganuma, K. Uniformly Connected Conductive Networks on Cellulose Nanofiber Paper for Transparent Paper Electronics. *NPG Asia Mater.* **2014**, *6*, No. e93.
(56) Koga, H.; Saito, T.; Kitaoka, T.; Nogi, M.; Suganuma, K.; Isogai, A. Transparent, Conductive, and Printable Composites Consisting of TEMPO-Oxidized Nanocellulose and Carbon Nanotube. *Biomacromolecules* **2013**, *14*, 1160−1165.
(57) Wu, H.; Kong, D.; Ruan, Z.; Hsu, P.-C.; Wang, S.; Yu, Z.; Carney, T. J.; Hu, L.; Fan, S.; Cui, Y. A Transparent Electrode Based on a Metal Nanotrough Network. *Nat. Nanotechnol.* **2013**, *8*, 421−425.
(58) Gao, K.; Shao, Z.; Wu, X.; Wang, X.; Li, J.; Zhang, Y.; Wang, W.; Wang, F. Cellulose Nanofibers/reduced Graphene Oxide Flexible Transparent Conductive Paper. *Carbohydr. Polym.* **2013**, *97*, 243−251.
(59) Pushparaj, V. L.; Shaijumon, M. M.; Kumar, A.; Murugesan, S.; Ci, L.; Vajtai, R.; Linhardt, R. J.; Nalamasu, O.; Ajayan, P. M. Flexible Energy Storage Devices Based on Nanocomposite Paper. *Proc. Natl. Acad. Sci. U. S. A.* **2007**, *104*, 13574−13577.
(60) He, S.; Hu, C.; Hou, H.; Chen, W. Ultrathin MnO2 Nanosheets Supported on Cellulose Based Carbon Papers for High-Power Supercapacitors. *J. Power Sources* **2014**, *246*, 754−761.
(61) Feng, J.-X.; Li, Q.; Lu, X.-F.; Tong, Y.-X.; Li, G.-R. Flexible Symmetrical Planar Supercapacitors Based on Multi-Layered MnO2/Ni/graphite/paper Electrodes with High-Efficient Electrochemical Energy Storage. *J. Mater. Chem. A* **2014**, *2*, 2985−2992.
(62) Lyu, S.; Chang, H.; Fu, F.; Hu, L.; Huang, J.; Wang, S. Cellulose-Coupled Graphene/polypyrrole Composite Electrodes Containing Conducting Networks Built by Carbon Fibers as Wearable Supercapacitors with Excellent Foldability and Tailorability. *J. Power Sources* **2016**, *327*, 438−446.
(63) Ren, G.; Li, S.; Fan, Z.-X.; Hoque, M. N. F.; Fan, Z. Ultrahigh-Rate Supercapacitors with Large Capacitance Based on Edge Oriented Graphene Coated Carbonized Cellulous Paper as Flexible Free-standing Electrodes. *J. Power Sources* **2016**, *325*, 152−160.
(64) Yan, J.; Yan, M.; Ge, L.; Yu, J.; Ge, S.; Huang, J. A Microfluidic Origami Electrochemiluminescence Aptamer-Device Based on a Porous Au-Paper Electrode and a Phenyleneethynylene Derivative. *Chem. Commun.* **2013**, *49*, 1383−1385.
(65) Feng, J.-X.; Ye, S.-H.; Lu, X.-F.; Tong, Y.-X.; Li, G.-R. Asymmetric Paper Supercapacitor Based on Amorphous Porous Mn3O4 Negative Electrode and Ni(OH)2 Positive Electrode: A Novel and High-Performance Flexible Electrochemical Energy Storage Device. *ACS Appl. Mater. Interfaces* **2015**, *7*, 11444−11451.
(66) Glatzel, S.; Schnepp, Z.; Giordano, C. From Paper to Structured Carbon Electrodes by Inkjet Printing. *Angew. Chem., Int. Ed.* **2013**, *52*, 2355−2358.
(67) Nogi, M.; Karakawa, M.; Komoda, N.; Yagyu, H.; Nge, T. T. Transparent Conductive Nanofiber Paper for Foldable Solar Cells. *Sci. Rep.* **2015**, *5*, 17254.
(68) Ahn, J.; Seo, J.-W.; Lee, T.-I.; Kwon, D.; Park, I.; Kim, T.-S.; Lee, J.-Y. Extremely Robust and Patternable Electrodes for Copy-Paper-Based Electronics. *ACS Appl. Mater. Interfaces* **2016**, *8*, 19031−19037.
(69) Wang, F.; Mao, P.; He, H. Dispensing of High Concentration Ag Nano-Particles Ink for Ultra-Low Resistivity Paper-Based Writing Electronics. *Sci. Rep.* **2016**, *6*, 21398.
(70) Xu, X.; Zhou, J.; Jiang, L.; Lubineau, G.; Ng, T.; Ooi, B. S.; Liao, H.-Y.; Shen, C.; Chen, L.; Zhu, J. Y. Highly Transparent, Low-Haze, Hybrid Cellulose Nanopaper as Electrodes for Flexible Electronics. *Nanoscale* **2016**, *8*, 12294−12306.
(71) Yao, Y.; Tao, J.; Zou, J.; Zhang, B.; Li, T.; Dai, J.; Zhu, M.; Wang, S.; Fu, K. K.; Henderson, D.; Hitz, E.; Peng, J.; Hu, L. Light Management in Plastic-Paper Hybrid Substrate Towards High-Performance Optoelectronics. *Energy Environ. Sci.* **2016**, *9*, 2278−2285.
(72) Asadpoordarvish, A.; Sandström, A.; Larsen, C.; Bollström, R.; Toivakka, M.; Österbacka, R.; Edman, L. Light-emitting Paper. *Adv. Funct. Mater.* **2015**, *25*, 3238−3245.
(73) Wang, T.; Zhang, Y.; Yan, Y.; Jones, C. G.; Lidzey, D. G. Polymer Light Emitting Diodes Powered via Paper-Mounted Electronics. *J. Disp. Technol.* **2016**, *12*, 583−588.
(74) Gomez, E. F.; Steckl, A. J. Improved Performance of OLEDs on Cellulose/Epoxy Substrate Using Adenine as a Hole Injection Layer. *ACS Photonics* **2015**, *2*, 439−445.
(75) Najafabadi, E.; Zhou, Y. H.; Knauer, K. A.; Fuentes-Hernandez, C.; Kippelen, B. Efficient Organic Light-Emitting Diodes Fabricated on Cellulose Nanocrystal Substrates. *Appl. Phys. Lett.* **2014**, *105*, 063305.
(76) Purandare, S.; Gomez, E. F.; Steckl, A. J. High Brightness Phosphorescent Organic Light Emitting Diodes on Transparent and Flexible Cellulose Films. *Nanotechnology* **2014**, *25*, 094012.
(77) Zhu, H.; Xiao, Z.; Liu, D.; Li, Y.; Weadock, N. J.; Fang, Z.; Huang, J.; Hu, L. Biodegradable Transparent Substrates for Flexible Organic-Light-Emitting Diodes. *Energy Environ. Sci.* **2013**, *6*, 2105−2111.
(78) Min, S.-H.; Kim, C. K.; Lee, H.-N.; Moon, D.-G. An OLED Using Cellulose Paper as a Flexible Substrate. *Mol. Cryst. Liq. Cryst.* **2012**, *563*, 159−165.
(79) Ummartyotin, S.; Juntaro, J.; Sain, M.; Manuspiya, H. Development of Transparent Bacterial Cellulose Nanocomposite Film as Substrate for Flexible Organic Light Emitting Diode (oled) Display. *Ind. Crops Prod.* **2012**, *35*, 92−97.
(80) Okahisa, Y.; Yoshida, A.; Miyaguchi, S.; Yano, H. Optically Transparent Wood−Cellulose Nanocomposite as a Base Substrate for Flexible Organic Light-Emitting Diode Displays. *Compos. Sci. Technol.* **2009**, *69*, 1958−1961.
(81) Legnani, C.; Vilani, C.; Calil, V. L.; Barud, H. S.; Quirino, W. G.; Achete, C. A.; Ribeiro, S. J. L.; Cremona, M. Bacterial Cellulose Membrane as Flexible Substrate for Organic Light Emitting Devices. *Thin Solid Films* **2008**, *517*, 1016−1020.
(82) Mazzeo, A. D.; Kalb, W. B.; Chan, L.; Killian, M. G.; Bloch, J.-F.; Mazzeo, B. A.; Whitesides, G. M. Paper-based, Capacitive Touch Pads. *Adv. Mater.* **2012**, *24*, 2850−2856.
(83) Wehrspohn, R. B.; Rau, U.; Gombert, A. *Photon Management in Solar Cells*; John Wiley & Sons, 2016.
(84) Priyadarshini, B. G.; Sharma, A. K. Design of Multi-Layer Anti-Reflection Coating for Terrestrial Solar Panel Glass. *Bull. Mater. Sci.* **2016**, *39*, 683−689.
(85) *ASTM D1003-13, Standard Test Method for Haze and Luminous Transmittance of Transparent Plastics*; ASTM International: West Conshohocken, PA, 2013; www.astm.org.
(86) Han, Z. W.; Wang, Z.; Feng, X. M.; Li, B.; Mu, Z. Z.; Zhang, J. Q.; Niu, S. C.; Ren, L. Q. Antireflective Surface Inspired from Biology: A Review. *Biosurface and Biotribology* **2016**, *2*, 137−150.
(87) Dellieu, L.; Sarrazin, M.; Simonis, P.; Deparis, O.; Vigneron, J. P. A Two-In-One Superhydrophobic and Anti-Reflective Nanodevice in the Grey Cicada Cicada Orni (hemiptera). *J. Appl. Phys.* **2014**, *116*, 024701.
(88) Miller, J. C. Reflection Efficiencies of a Periodic Absorbing Surface. *J. Opt. Soc. Am.* **1964**, *54*, 353−356.
(89) Clapham, P. B.; Hutley, M. C. Reduction of Lens Reflexion by the "moth Eye" Principle. *Nature* **1973**, *244*, 281.
(90) Wilson, S. J.; Hutley, M. C. The Optical Properties of 'moth Eye' Antireflection Surfaces. *Opt. Acta* **1982**, *29*, 993−1009.

https://dx.doi.org/10.1021/acsnano.0c06452
ACS Nano XXXX, XXX, XXX−XXX

(91) Bernhard, C. Structural and Functional Adaptation in a Visual System. *Endeavour* **1967**, *26*, 79−84.
(92) Johnsen, S. Hidden in Plain Sight: The Ecology and Physiology of Organismal Transparency. *Biol. Bull.* **2001**, *201*, 301−318.
(93) Binetti, V. R.; Schiffman, J. D.; Leaffer, O. D.; Spanier, J. E.; Schauer, C. L. The Natural Transparency and Piezoelectric Response of the Greta Oto Butterfly Wing. *Integrative Biology* **2009**, *1*, 324−329.
(94) Yoshida, A.; Motoyama, M.; Kosaku, A.; Miyamoto, K. Antireflective Nanoprotuberance Array in the Transparent Wing of a Hawkmoth, Cephonodes Hylas. *Zool. Sci.* **1997**, *14*, 737−741.
(95) Zhang, G.; Zhang, J.; Xie, G.; Liu, Z.; Shao, H. Cicada Wings: A Stamp from Nature for Nanoimprint Lithography. *Small* **2006**, *2*, 1440−1443.
(96) Wang, B.; Gao, T.; Leu, P. W. Computational Simulations of Nanostructured Solar Cells. *Nano LIFE* **2012**, *02*, 1230007.
(97) Yeh, P. *Optical Waves in Layered Media*, 2nd ed.; Wiley: Hoboken, NJ, 2005.
(98) Haghanifar, S.; McCourt, M.; Cheng, B.; Wuenschell, J.; Ohodnicki, P.; Leu, P. W. Discovering High-Performance Broadband and Broad Angle Antireflection Surfaces by Machine Learning. *Optica* **2020**, *7*, 784−789.
(99) Rayleigh, L. On Reflection of Vibrations at the Confines of Two Media Between Which the Transition Is Gradual. *Proceedings of the London Mathematical Society* **1879**, *s1−11*, 51−56.
(100) Han, Z.; Jiao, Z.; Niu, S.; Ren, L. Ascendant Bioinspired Antireflective Materials: Opportunities and Challenges Coexist. *Prog. Mater. Sci.* **2019**, *103*, 1−68.
(101) Li, Y.; Zhang, J.; Yang, B. Antireflective Surfaces Based on Biomimetic Nanopillared Arrays. *Nano Today* **2010**, *5*, 117−127.
(102) Cai, J.; Qi, L. Recent Advances in Antireflective Surfaces Based on Nanostructure Arrays. *Mater. Horiz.* **2015**, *2*, 37−53.
(103) Yao, L.; He, J. Recent Progress in Antireflection and Self-Cleaning Technology − From Surface Engineering to Functional Surfaces. *Prog. Mater. Sci.* **2014**, *61*, 94−143.
(104) Tan, G.; Lee, J.-H.; Lan, Y.-H.; Wei, M.-K.; Peng, L.-H.; Cheng, I.-C.; Wu, S.-T. Broadband Antireflection Film with Moth-Eye-Like Structure for Flexible Display Applications. *Optica* **2017**, *4*, 678−683.
(105) Ji, S.; Song, K.; Nguyen, T. B.; Kim, N.; Lim, H. Optimal Moth Eye Nanostructure Array on Transparent Glass Towards Broadband Antireflection. *ACS Appl. Mater. Interfaces* **2013**, *5*, 10731−10737.
(106) Ye, X.; Huang, J.; Geng, F.; Sun, L.; Liu, H.; Jiang, X.; Wu, W.; Zu, X.; Zheng, W. Broadband Antireflection Subwavelength Structures on Fused Silica Using Lower Temperatures Normal Atmosphere Thermal Dewetted Au Nanopatterns. *IEEE Photonics J.* **2016**, *8*, 1−10.
(107) van de Groep, J.; Gupta, D.; Verschuuren, M. A.; Wienk, M. M.; Janssen, R. A. J.; Polman, A. Large-Area Soft-Imprinted Nanowire Networks as Light Trapping Transparent Conductors. *Sci. Rep.* **2015**, *5*, 11414.
(108) Zhang, C.; Li, W.; Yu, D.; Wang, Y.; Yin, M.; Wang, H.; Song, Y.; Zhu, X.; Chang, P.; Chen, X.; Li, D. Wafer-scale Highly Ordered Anodic Aluminum Oxide by Soft Nanoimprinting Lithography for Optoelectronics Light Management. *Adv. Mater. Interfaces* **2017**, *4*, 1601116.
(109) Jin, B.; He, J. Self-templated Fabrication of Robust Moth-Eye-Like Nanostructures with Broadband and Quasi-Omnidirectional Antireflection Properties. *ACS Photonics* **2017**, *4*, 188−196.
(110) Infante, D.; Koch, K. W.; Mazumder, P.; Tian, L.; Carrilero, A.; Tulli, D.; Baker, D.; Pruneri, V. Durable, Superhydrophobic, Antireflection, and Low Haze Glass Surfaces Using Scalable Metal Dewetting Nanostructuring. *Nano Res.* **2013**, *6*, 429−440.
(111) *Solar Spectral Irradiance: Air Mass 1.5*; http://rredc.nrel.gov/solar/spectra/am1.5/.
(112) Yee, K. Numerical Solution of Initial Boundary Value Problems Involving Maxwell's Equations in Isotropic Media. *IEEE Trans. Antennas Propag.* **1966**, *14*, 302−307.
(113) Jeong, S.; Hu, L.; Lee, H. R.; Garnett, E.; Choi, J. W.; Cui, Y. Fast and Scalable Printing of Large Area Monolayer Nanoparticles for Nanotexturing Applications. *Nano Lett.* **2010**, *10*, 2989−2994.
(114) Kang, G.; Park, H.; Shin, D.; Baek, S.; Choi, M.; Yu, D.-H.; Kim, K.; Padilla, W. J. Broadband Light-Trapping Enhancement in an Ultrathin Film A-Si Absorber Using Whispering Gallery Modes and Guided Wave Modes with Dielectric Surface-Textured Structures. *Adv. Mater.* **2013**, *25*, 2617−2623.
(115) Gao, T.; Haghanifar, S.; Lindsay, M. G.; Lu, P.; Kayes, M. I.; Pafchek, B. D.; Zhou, Z.; Ohodnicki, P. R.; Leu, P. W. Fundamental Performance Limits and Haze Evaluation of Metal Nanomesh Transparent Conductors. *Adv. Opt. Mater.* **2018**, *6*, 1700829.
(116) Siró, I.; Plackett, D.; Hedenqvist, M.; Ankerfors, M.; Lindström, T. Highly Transparent Films from Carboxymethylated Microfibrillated Cellulose: The Effect of Multiple Homogenization Steps on Key Properties. *J. Appl. Polym. Sci.* **2011**, *119*, 2652−2660.
(117) Zhu, H.; Parvinian, S.; Preston, C.; Vaaland, O.; Ruan, Z.; Hu, L. Transparent Nanopaper with Tailored Optical Properties. *Nanoscale* **2013**, *5*, 3787−3792.
(118) Fang, Z.; Zhu, H.; Bao, W.; Preston, C.; Liu, Z.; Dai, J.; Li, Y.; Hu, L. Highly Transparent Paper with Tunable Haze for Green Electronics. *Energy Environ. Sci.* **2014**, *7*, 3313−3319.
(119) Zhu, M.; Li, T.; Davis, C. S.; Yao, Y.; Dai, J.; Wang, Y.; AlQatari, F.; Gilman, J. W.; Hu, L. Transparent and Haze Wood Composites for Highly Efficient Broadband Light Management in Solar Cells. *Nano Energy* **2016**, *26*, 332−339.
(120) Zhu, H.; Fang, Z.; Wang, Z.; Dai, J.; Yao, Y.; Shen, F.; Preston, C.; Wu, W.; Peng, P.; Jang, N.; Yu, Q.; Yu, Z.; Hu, L. Extreme Light Management in Mesoporous Wood Cellulose Paper for Optoelectronics. *ACS Nano* **2016**, *10*, 1369−1377.
(121) Zhu, M.; Li, T.; Davis, C. S.; Yao, Y.; Dai, J.; Wang, Y.; AlQatari, F.; Gilman, J. W.; Hu, L. Transparent and Haze Wood Composites for Highly Efficient Broadband Light Management in Solar Cells. *Nano Energy* **2016**, *26*, 332−339.
(122) Kang, G.; Bae, K.; Nam, M.; Ko, D.-H.; Kim, K.; Padilla, W. J. Broadband and Ultrahigh Optical Haze Thin Films with Self-Aggregated Alumina Nanowire Bundles for Photovoltaic Applications. *Energy Environ. Sci.* **2015**, *8*, 2650−2656.
(123) Chu, W.-P.; Lin, J.-S.; Lin, T.-C.; Tsai, Y.-S.; Kuo, C.-W.; Chung, M.-H.; Hsieh, T.-E.; Liu, L.-C.; Juang, F.-S.; Chen, N.-P. Using High Haze (>90%) Light-Trapping Film to Enhance the Efficiency of A-si:h Solar Cells. *Opt. Commun.* **2012**, *285*, 3325−3328.
(124) Yun, J.; Wang, W.; Kim, S. M.; Bae, T.-S.; Lee, S.; Kim, D.; Lee, G.-H.; Lee, H.-S.; Song, M. Light Trapping in Bendable Organic Solar Cells Using Silica Nanoparticle Arrays. *Energy Environ. Sci.* **2015**, *8*, 932−940.
(125) Liu, X.; Xiong, Y.; Shen, J.; Guo, S. Fast Fabrication of a Novel Transparent PMMA Light Scattering Materials with High Haze by Doping with Ordinary Polymer. *Opt. Express* **2015**, *23*, 17793−17804.
(126) Liu, X.; Zhao, Z.; Xiong, Y.; Yi, P.; Guo, S. Cost-Effective Way to Improve the Optical Properties of Poly(methyl Methacrylate)/poly(ethylene Terephthalate) Light Scattering Materials: Drop Coalescence. *Appl. Opt.* **2018**, *57*, 2107−2114.
(127) Kayes, M. I.; Galante, A. J.; Stella, N. A.; Haghanifar, S.; Shanks, R. M.; Leu, P. W. Stable Lotus Leaf-Inspired Hierarchical, Fluorinated Polypropylene Surfaces for Reduced Bacterial Adhesion. *React. Funct. Polym.* **2018**, *128*, 40−46.
(128) Galante, A. J.; Haghanifar, S.; Romanowski, E. G.; Shanks, R. M. Q.; Leu, P. W. Superhemophobic and Antivirofouling Coating for Mechanically Durable and Wash-Stable Medical Textiles. *ACS Appl. Mater. Interfaces* **2020**, *12*, 22120−22128.
(129) Genzer, J.; Efimenko, K. Recent Developments in Superhydrophobic Surfaces and Their Relevance to Marine Fouling: a Review. *Biofouling* **2006**, *22*, 339−360.
(130) Teisala, H.; Tuominen, M.; Kuusipalo, J. Superhydrophobic Coatings on Cellulose-Based Materials: Fabrication, Properties, and Applications. *Adv. Mater. Interfaces* **2014**, *1*, 1300026.

https://dx.doi.org/10.1021/acsnano.0c06452
ACS Nano XXXX, XXX, XXX−XXX

(131) Roach, P.; Shirtcliffe, N. J.; Newton, M. I. Progess in Superhydrophobic Surface Development. *Soft Matter* **2008**, *4*, 224−240.
(132) Young, T., III An Essay on the Cohesion of Fluids. *Philosophical Transactions of the Royal Society of London* **1805**, *95*, 65−87.
(133) Wenzel, R. N. Resistance of Solid Surfaces to Wetting by Water. *Ind. Eng. Chem.* **1936**, *28*, 988−994.
(134) Cassie, A. B. D.; Baxter, S. Wettability of Porous Surfaces. *Trans. Faraday Soc.* **1944**, *40*, 546.
(135) Seo, K.; Kim, M.; Kim, D. H. *Re-derivation of Young's Equation, Wenzel Equation, and Cassie-Baxter Equation Based on Energy Minimization*; Intech, 2015.
(136) Marmur, A. From Hygrophilic to Superhygrophobic: Theoretical Conditions for Making High-Contact-Angle Surfaces from Low-Contact-Angle Materials. *Langmuir* **2008**, *24*, 7573−7579.
(137) Chu, Z.; Seeger, S. Superamphiphobic Surfaces. *Chem. Soc. Rev.* **2014**, *43*, 2784−2798.
(138) Zheng, Q.-S.; Yu, Y.; Zhao, Z.-H. Effects of Hydraulic Pressure on the Stability and Transition of Wetting Modes of Superhydrophobic Surfaces. *Langmuir* **2005**, *21*, 12207−12212.
(139) Gao, L.; McCarthy, T. J. Contact Angle Hysteresis Explained. *Langmuir* **2006**, *22*, 6234−6237.
(140) Drelich, J.; Marmur, A. Physics and applications of superhydrophobic and superhydrophilic surfaces and coatings. *Surf. Innovations* **2014**, *2*, 211−227.
(141) Hensel, R.; Neinhuis, C.; Werner, C. The Springtail Cuticle as a Blueprint for Omniphobic Surfaces. *Chem. Soc. Rev.* **2016**, *45*, 323−341.
(142) Liu, M.; Zheng, Y.; Zhai, J.; Jiang, L. Bioinspired Super-Antiwetting Interfaces with Special Liquid-Solid Adhesion. *Acc. Chem. Res.* **2010**, *43*, 368−377.
(143) Yong, J.; Chen, F.; Yang, Q.; Zhang, D.; Farooq, U.; Du, G.; Hou, X. Bioinspired Underwater Superoleophobic Surface with Ultralow Oil-Adhesion Achieved by Femtosecond Laser Microfabrication. *J. Mater. Chem. A* **2014**, *2*, 8790−8795.
(144) Prum, R. O.; Quinn, T.; Torres, R. H. Anatomically Diverse Butterfly Scales All Produce Structural Colours by Coherent Scattering. *J. Exp. Biol.* **2006**, *209*, 748−765.
(145) Mouterde, T.; Lehoucq, G.; Xavier, S.; Checco, A.; Black, C. T.; Rahman, A.; Midavaine, T.; Clanet, C.; Quéré, D. Antifogging Abilities of Model Nanotextures. *Nat. Mater.* **2017**, *16*, 658−663.
(146) Wilke, K. L.; Preston, D. J.; Lu, Z.; Wang, E. N. Toward Condensation-Resistant Omniphobic Surfaces. *ACS Nano* **2018**, *12*, 11013−11021.
(147) Zhang, X.; Sato, O.; Taguchi, M.; Einaga, Y.; Murakami, T.; Fujishima, A. Self-Cleaning Particle Coating with Antireflection Properties. *Chem. Mater.* **2005**, *17*, 696−700.
(148) Zhang, G.; Wang, D.; Gu, Z.; Möhwald, H. Fabrication of Superhydrophobic Surfaces from Binary Colloidal Assembly. *Langmuir* **2005**, *21*, 9143−9148.
(149) Ling, X. Y.; Phang, I. Y.; Vancso, G. J.; Huskens, J.; Reinhoudt, D. N. Stable and Transparent Superhydrophobic Nanoparticle Films. *Langmuir* **2009**, *25*, 3260−3263.
(150) Darmanin, T.; Guittard, F. Superhydrophobic and Superoleophobic Properties in Nature. *Mater. Today* **2015**, *18*, 273−285.
(151) Barthlott, W.; Neinhuis, C. Purity of the Sacred Lotus, or Escape from Contamination in Biological Surfaces. *Planta* **1997**, *202*, 1−8.
(152) Cheng, Y. T.; Rodak, D. E.; Wong, C. A.; Hayden, C. A. Effects of Micro- and Nano-Structures on the Self-Cleaning Behaviour of Lotus Leaves. *Nanotechnology* **2006**, *17*, 1359−1362.
(153) Koch, K.; Ensikat, H.-J. The Hydrophobic Coatings of Plant Surfaces: Epicuticular Wax Crystals and Their Morphologies, Crystallinity and Molecular Self-Assembly. *Micron* **2008**, *39*, 759−772.
(154) Gu, Z.-Z.; Uetsuka, H.; Takahashi, K.; Nakajima, R.; Onishi, H.; Fujishima, A.; Sato, O. Structural Color and the Lotus Effect. *Angew. Chem., Int. Ed.* **2003**, *42*, 894−897.
(155) Perez Goodwyn, P.; Maezono, Y.; Hosoda, N.; Fujisaki, K. Waterproof and Translucent Wings at the Same Time: Problems and Solutions in Butterflies. *Naturwissenschaften* **2009**, *96*, 781−787.
(156) Bixler, G. D.; Bhushan, B. Rice- and Butterfly-Wing Effect Inspired Self-Cleaning and Low Drag Micro/nanopatterned Surfaces in Water, Oil, and Air Flow. *Nanoscale* **2014**, *6*, 76−96.
(157) Zheng, Y.; Gao, X.; Jiang, L. Directional Adhesion of Superhydrophobic Butterfly Wings. *Soft Matter* **2007**, *3*, 178−182.
(158) Nickerl, J.; Helbig, R.; Schulz, H.-J.; Werner, C.; Neinhuis, C. Diversity and Potential Correlations to the Function of Collembola Cuticle Structures. *Zoomorphology* **2013**, *132*, 183−195.
(159) Nickerl, J.; Tsurkan, M.; Hensel, R.; Neinhuis, C.; Werner, C. The Multi-Layered Protective Cuticle of Collembola: a Chemical Analysis. *J. R. Soc., Interface* **2014**, *11*, 20140619.
(160) Sahoo, B.; Yoon, K.; Seo, J.; Lee, T. Chemical and Physical Pathways for Fabricating Flexible Superamphiphobic Surfaces with High Transparency. *Coatings* **2018**, *8*, 47.
(161) Golovin, K.; Boban, M.; Mabry, J. M.; Tuteja, A. Designing Self-Healing Superhydrophobic Surfaces with Exceptional Mechanical Durability. *ACS Appl. Mater. Interfaces* **2017**, *9*, 11212−11223.
(162) Wang, H.; Zhou, H.; Gestos, A.; Fang, J.; Lin, T. Robust, Superamphiphobic Fabric with Multiple Self-Healing Ability Against Both Physical and Chemical Damages. *ACS Appl. Mater. Interfaces* **2013**, *5*, 10221−10226.
(163) Yong, J.; Chen, F.; Yang, Q.; Huo, J.; Hou, X. Superoleophobic Surfaces. *Chem. Soc. Rev.* **2017**, *46*, 4168−4217.
(164) Hare, E. F.; Shafrin, E. G.; Zisman, W. A. Properties of Films of Adsorbed Fluorinated Acids. *J. Phys. Chem.* **1954**, *58*, 236−239.
(165) Nishino, T.; Meguro, M.; Nakamae, K.; Matsushita, M.; Ueda, Y. The Lowest Surface Free Energy Based on -cf $_3$ Alignment. *Langmuir* **1999**, *15*, 4321−4323.
(166) Wang, H.; Xue, Y.; Ding, J.; Feng, L.; Wang, X.; Lin, T. Durable, Self-Healing Superhydrophobic and Superoleophobic Surfaces from Fluorinated-Decyl Polyhedral Oligomeric Silsesquioxane and Hydrolyzed Fluorinated Alkyl Silane. *Angew. Chem.* **2011**, *123*, 11635−11638.
(167) Golovin, K.; Lee, D. H.; Mabry, J. M.; Tuteja, A. Transparent, Flexible, Superomniphobic Surfaces with Ultra-Low Contact Angle Hysteresis. *Angew. Chem., Int. Ed.* **2013**, *52*, 13007−13011.
(168) Pan, S.; Kota, A. K.; Mabry, J. M.; Tuteja, A. Superomniphobic Surfaces for Effective Chemical Shielding. *J. Am. Chem. Soc.* **2013**, *135*, 578−581.
(169) Lin, A. Y.-C.; Panchangam, S. C.; Tsai, Y.-T.; Yu, T.-H. Occurrence of Perfluorinated Compounds in the Aquatic Environment as Found in Science Park Effluent, River Water, Rainwater, Sediments, and Biotissues. *Environ. Monit. Assess.* **2014**, *186*, 3265−3275.
(170) Perkola, N.; Sainio, P. Survey of Perfluorinated Alkyl Acids in Finnish Effluents, Storm Water, Landfill Leachate and Sludge. *Environ. Sci. Pollut. Res.* **2013**, *20*, 7979−7987.
(171) DeWitt, J. C., Ed. *Toxicological Effects of Perfluoroalkyl and Polyfluoroalkyl Substances; Molecular and Integrative Toxicology*; Springer International Publishing: Cham, 2015.
(172) Martin, J. W.; Kannan, K.; Berger, U.; Voogt, P. D.; Field, J.; Franklin, J.; Giesy, J. P.; Harner, T.; Muir, D. C. G.; Scott, B.; Kaiser, M.; Järnberg, U.; Jones, K. C.; Mabury, S. A.; Schroeder, H.; Simcik, M.; Sottani, C.; Bavel, B. V.; Kärrman, A.; Lindström, G.; et al. Peer Reviewed: Analytical Challenges Hamper Perfluoroalkyl Research. *Environ. Sci. Technol.* **2004**, *38*, 248A−255A.
(173) Lau, C.; Butenhoff, J. L.; Rogers, J. M. The Developmental Toxicity of Perfluoroalkyl Acids and Their Derivatives. *Toxicol. Appl. Pharmacol.* **2004**, *198*, 231−241.
(174) Schellenberger, S.; Gillgard, P.; Stare, A.; Hanning, A.; Levenstam, O.; Roos, S.; Cousins, I. T. Facing the Rain After the Phase Out: Performance Evaluation of Alternative Fluorinated and Non-Fluorinated Durable Water Repellents for Outdoor Fabrics. *Chemosphere* **2018**, *193*, 675−684.
(175) Schellenberger, S.; Hill, P. J.; Levenstam, O.; Gillgard, P.; Cousins, I. T.; Taylor, M.; Blackburn, R. S. Highly Fluorinated

https://dx.doi.org/10.1021/acsnano.0c06452
ACS Nano XXXX, XXX, XXX−XXX

Chemicals in Functional Textiles Can Be Replaced by Re-Evaluating Liquid Repellency and End-User Requirements. *J. Cleaner Prod.* **2019**, *217*, 134−143.
(176) Tuteja, A.; Choi, W.; Ma, M.; Mabry, J. M.; Mazzella, S. A.; Rutledge, G. C.; McKinley, G. H.; Cohen, R. E. Designing Superoleophobic Surfaces. *Science* **2007**, *318*, 1618−1622.
(177) Nosonovsky, M.; Bhushan, B. Why Re-Entrant Surface Topography Is Needed for Robust Oleophobicity. *Philos. Trans. R. Soc., A* **2016**, *374*, 20160185.
(178) Nosonovsky, M. Multiscale Roughness and Stability of Superhydrophobic Biomimetic Interfaces. *Langmuir* **2007**, *23*, 3157−3161.
(179) Michielsen, S.; Lee, H. J. Design of a Superhydrophobic Surface Using Woven Structures. *Langmuir* **2007**, *23*, 6004−6010.
(180) Kleingartner, J. A.; Srinivasan, S.; Truong, Q. T.; Sieber, M.; Cohen, R. E.; McKinley, G. H. Designing Robust Hierarchically Textured Oleophobic Fabrics. *Langmuir* **2015**, *31*, 13201−13213.
(181) Whyman, G.; Bormashenko, E. How to Make a Cassie Wetting State Stable? *Langmuir* **2011**, *27*, 8171−8176.
(182) Hensel, R.; Helbig, R.; Aland, S.; Braun, H.-G.; Voigt, A.; Neinhuis, C.; Werner, C. Wetting Resistance at Its Topographical Limit: The Benefit of Mushroom and Serif T Structures. *Langmuir* **2013**, *29*, 1100−1112.
(183) Choi, J.; Jo, W.; Lee, S. Y.; Jung, Y. S.; Kim, S.-H.; Kim, H.-T. Flexible and Robust Superomniphobic Surfaces Created by Localized Photofluidization of Azopolymer Pillars. *ACS Nano* **2017**, *11*, 7821−7828.
(184) Liu, T. L.; Kim, C.-J. C. Turning a Surface Superrepellent Even to Completely Wetting Liquids. *Science* **2014**, *346*, 1096−1100.
(185) Domingues, E. M.; Arunachalam, S.; Mishra, H. Doubly Reentrant Cavities Prevent Catastrophic Wetting Transitions on Intrinsically Wetting Surfaces. *ACS Appl. Mater. Interfaces* **2017**, *9*, 21532−21538.
(186) Liu, X.; Gu, H.; Wang, M.; Du, X.; Gao, B.; Elbaz, A.; Sun, L.; Liao, J.; Xiao, P.; Gu, Z. 3d Printing of Bioinspired Liquid Superrepellent Structures. *Adv. Mater.* **2018**, *30*, 1800103.
(187) Jang, G. G.; Smith, D. B.; Polizos, G.; Collins, L.; Keum, J. K.; Lee, D. F. Transparent Superhydrophilic and Superhydrophobic Nanoparticle Textured Coatings: Comparative Study of Anti-Soiling Performance. *Nanoscale Adv.* **2019**, *1*, 1249−1260.
(188) Kirschner, C. M.; Brennan, A. B. Bio-Inspired Antifouling Strategies. *Annu. Rev. Mater. Res.* **2012**, *42*, 211−229.
(189) Scardino, A. J.; Hudleston, D.; Peng, Z.; Paul, N. A.; de Nys, R. Biomimetic Characterisation of Key Surface Parameters for the Development of Fouling Resistant Materials. *Biofouling* **2009**, *25*, 83−93.
(190) Bahattab, M. A.; Alhomoudi, I. A.; Alhussaini, M. I.; Mirza, M.; Hegmann, J.; Glaubitt, W.; Löbmann, P. Anti-Soiling Surfaces for PV Applications Prepared by Sol-Gel Processing: Comparison of Laboratory Testing and Outdoor Exposure. *Sol. Energy Mater. Sol. Cells* **2016**, *157*, 422−428.
(191) Ragesh, P.; Anand Ganesh, V.; Nair, S. V.; Nair, A. S. A Review on 'self-Cleaning and Multifunctional Materials'. *J. Mater. Chem. A* **2014**, *2*, 14773−14797.
(192) Gao, L.; McCarthy, T. J. The "lotus Effect" Explained: Two Reasons Why Two Length Scales of Topography Are Important. *Langmuir* **2006**, *22*, 2966−2967.
(193) Von Baeyer, H. C. The Lotus Effect. *Sciences* **2000**, *40*, 12−15.
(194) Ilse, K.; Figgis, B.; Khan, M. Z.; Naumann, V.; Hagendorf, C. Dew as a Detrimental Influencing Factor for Soiling of Pv Modules. *IEEE Journal of Photovoltaics* **2019**, *9*, 287−294.
(195) Haghanifar, S.; Tomasovic, L. M.; Galante, A. J.; Pekker, D.; Leu, P. W. Stain-Resistant, Superomniphobic Flexible Optical Plastics Based on Nano-Enoki Mushroom-Like Structures. *J. Mater. Chem. A* **2019**, *7*, 15698−15706.
(196) Bayer, I. S. On the Durability and Wear Resistance of Transparent Superhydrophobic Coatings. *Coatings* **2017**, *7*, 12.
(197) Jung, Y. C.; Bhushan, B. Wetting Behaviour During Evaporation and Condensation of Water Microdroplets on Superhydrophobic Patterned Surfaces. *J. Microsc.* **2008**, *229*, 127−140.
(198) Dorrer, C.; Rühe, J. Condensation and Wetting Transitions on Microstructured Ultrahydrophobic Surfaces. *Langmuir* **2007**, *23*, 3820−3824.
(199) Wier, K. A.; McCarthy, T. J. Condensation on Ultrahydrophobic Surfaces and Its Effect on Droplet Mobility: Ultrahydrophobic Surfaces Are Not Always Water Repellant. *Langmuir* **2006**, *22*, 2433−2436.
(200) Rykaczewski, K.; Paxson, A. T.; Staymates, M.; Walker, M. L.; Sun, X.; Anand, S.; Srinivasan, S.; McKinley, G. H.; Chinn, J.; Scott, J. H. J.; Varanasi, K. K. Dropwise Condensation of Low Surface Tension Fluids on Omniphobic Surfaces. *Sci. Rep.* **2015**, *4*, 4158.
(201) Lafuma, A.; Quere, D. Superhydrophobic States. *Nat. Mater.* **2003**, *2*, 457−460.
(202) Liu, Y.; Chen, X.; Xin, J. H. Can Superhydrophobic Surfaces Repel Hot Water? *J. Mater. Chem.* **2009**, *19*, 5602−5611.
(203) Gao, X.; Yan, X.; Yao, X.; Xu, L.; Zhang, K.; Zhang, J.; Yang, B.; Jiang, L. The Dry-Style Antifogging Properties of Mosquito Compound Eyes and Artificial Analogues Prepared by Soft Lithography. *Adv. Mater.* **2007**, *19*, 2213−2217.
(204) Wisdom, K. M.; Watson, J. A.; Qu, X.; Liu, F.; Watson, G. S.; Chen, C.-H. Self-Cleaning of Superhydrophobic Surfaces by Self-Propelled Jumping Condensate. *Proc. Natl. Acad. Sci. U. S. A.* **2013**, *110*, 7992−7997.
(205) Lee, D.; Rubner, M. F.; Cohen, R. E. All-nanoparticle Thin-Film Coatings. *Nano Lett.* **2006**, *6*, 2305−2312.
(206) Miyauchi, M.; Nakajima, A.; Hashimoto, K.; Watanabe, T. A Highly Hydrophilic Thin Film Under 1 $\mu w/cm^2$ UV Illumination. *Adv. Mater.* **2000**, *12*, 1923−1927.
(207) Wang, R.; Hashimoto, K.; Fujishima, A.; Chikuni, M.; Kojima, E.; Kitamura, A.; Shimohigoshi, M.; Watanabe, T. Light-Induced Amphiphilic Surfaces. *Nature* **1997**, *388*, 431.
(208) Grosu, G.; Andrzejewski, L.; Veilleux, G.; Ross, G. G. Relation Between the Size of Fog Droplets and Their Contact Angles with CR39 Surfaces. *J. Phys. D: Appl. Phys.* **2004**, *37*, 3350−3355.
(209) Cebeci, F. Ç.; Wu, Z.; Zhai, L.; Cohen, R. E.; Rubner, M. F. Nanoporosity-driven Superhydrophilicity: A Means to Create Multifunctional Antifogging Coatings. *Langmuir* **2006**, *22*, 2856−2862.
(210) Varshney, P.; Mohapatra, S. S. Durable and Regenerable Superhydrophobic Coatings for Brass Surfaces with Excellent Self-Cleaning and Anti-Fogging Properties Prepared by Immersion Technique. *Tribol. Int.* **2018**, *123*, 17−25.
(211) Cao, L.; White, J. S.; Park, J.; Schuller, J. A.; Clemens, B. M.; Brongersma, M. L. Engineering Light Absorption in Semiconductor Nanowire Devices. *Nat. Mater.* **2009**, *8*, 643−647.
(212) Campbell, J. M.; Meldrum, F. C.; Christenson, H. K. Observing the Formation of Ice and Organic Crystals in Active Sites. *Proc. Natl. Acad. Sci. U. S. A.* **2017**, *114*, 810−815.
(213) Meuler, A. J.; McKinley, G. H.; Cohen, R. E. Exploiting Topographical Texture To Impart Icephobicity. *ACS Nano* **2010**, *4*, 7048−7052.
(214) Wang, N.; Xiong, D.; Pan, S.; Wang, K.; Shi, Y.; Deng, Y. Robust Superhydrophobic Coating and the Anti-Icing Properties of Its Lubricants-Infused-Composite Surface Under Condensing Condition. *New J. Chem.* **2017**, *41*, 1846−1853.
(215) Chatterjee, R.; Beysens, D.; Anand, S. Delaying Ice and Frost Formation Using Phase-Switching Liquids. *Adv. Mater.* **2019**, *31*, 1807812.
(216) Wang, H.; He, M.; Liu, H.; Guan, Y. One-step Fabrication of Robust Superhydrophobic Steel Surfaces with Mechanical Durability, Thermal Stability, and Anti-Icing Function. *ACS Appl. Mater. Interfaces* **2019**, *11*, 25586−25594.
(217) Leijtens, T.; Eperon, G. E.; Pathak, S.; Abate, A.; Lee, M. M.; Snaith, H. J. Overcoming Ultraviolet Light Instability of Sensitized TiO_2 with Meso-Superstructured Organometal Tri-Halide Perovskite Solar Cells. *Nat. Commun.* **2013**, *4*, 2885.

https://dx.doi.org/10.1021/acsnano.0c06452
ACS Nano XXXX, XXX, XXX−XXX

(218) Lee, J.-W.; Kim, D.-H.; Kim, H.-S.; Seo, S.-W.; Cho, S. M.; Park, N.-G. Formamidinium and Cesium Hybridization for Photo- and Moisture-Stable Perovskite Solar Cell. *Adv. Energy Mater.* **2015**, *5*, 1501310.
(219) Guarnera, S.; Abate, A.; Zhang, W.; Foster, J. M.; Richardson, G.; Petrozza, A.; Snaith, H. J. Improving the Long-Term Stability of Perovskite Solar Cells with a Porous Al2O3 Buffer Layer. *J. Phys. Chem. Lett.* **2015**, *6*, 432−437.
(220) Zhou, H.; Wang, H.; Niu, H.; Gestos, A.; Lin, T. Robust, Self-Healing Superamphiphobic Fabrics Prepared by Two-Step Coating of Fluoro-Containing Polymer, Fluoroalkyl Silane, and Modified Silica Nanoparticles. *Adv. Funct. Mater.* **2013**, *23*, 1664−1670.
(221) Zardetto, V.; Brown, T. M.; Reale, A.; Di Carlo, A. Substrates for Flexible Electronics: A Practical Investigation on the Electrical, Film Flexibility, Optical, Temperature, and Solvent Resistance Properties. *J. Polym. Sci., Part B: Polym. Phys.* **2011**, *49*, 638−648.
(222) Park, J. W.; Shin, D. C.; Park, S. H. Large-Area OLED Lightings and Their Applications. *Semicond. Sci. Technol.* **2011**, *26*, 034002.
(223) Lewis, J.; Weaver, M. Thin-Film Permeation-Barrier Technology for Flexible Organic Light-Emitting Devices. *IEEE J. Sel. Top. Quantum Electron.* **2004**, *10*, 45−57.
(224) Tseng, I.-H.; Liao, Y.-F.; Chiang, J.-C.; Tsai, M.-H. Transparent Polyimide/graphene Oxide Nanocomposite with Improved Moisture Barrier Property. *Mater. Chem. Phys.* **2012**, *136*, 247−253.
(225) Groten, J.; Rühe, J. Surfaces with Combined Microscale and Nanoscale Structures: A Route to Mechanically Stable Superhydrophobic Surfaces? *Langmuir* **2013**, *29*, 3765−3772.
(226) Milionis, A.; Loth, E.; Bayer, I. S. Recent Advances in the Mechanical Durability of Superhydrophobic Materials. *Adv. Colloid Interface Sci.* **2016**, *229*, 57−79.
(227) Tian, X.; Verho, T.; Ras, R. H. A. Moving Superhydrophobic Surfaces Toward Real-World Applications. *Science* **2016**, *352*, 142−143.
(228) Ellinas, K.; Tserepi, A.; Gogolides, E. Durable Superhydrophobic and Superamphiphobic Polymeric Surfaces and Their Applications: A Review. *Adv. Colloid Interface Sci.* **2017**, *250*, 132−157.
(229) Rahmawan, Y.; Xu, L.; Yang, S. Self-Assembly of Nanostructures Towards Transparent, Superhydrophobic Surfaces. *J. Mater. Chem. A* **2013**, *1*, 2955−2969.
(230) Barati Darband, G.; Aliofkhazraei, M.; Khorsand, S.; Sokhanvar, S.; Kaboli, A. Science and Engineering of Superhydrophobic Surfaces: Review of Corrosion Resistance, Chemical and Mechanical Stability. *Arabian J. Chem.* **2020**, *13*, 1763−1802.
(231) Fu, Q.; Tang, X.; Huang, B.; Hu, T.; Tan, L.; Chen, L.; Chen, Y. Recent Progress on the Long-Term Stability of Perovskite Solar Cells. *Adv. Sci.* **2018**, *5*, 1700387.
(232) Garner, S.; Glaesemann, S.; Li, X. Ultra-Slim Flexible Glass for Roll-To-Roll Electronic Device Fabrication. *Appl. Phys. A: Mater. Sci. Process.* **2014**, *116*, 403−407.
(233) Jenkins, W. Glass in Electronics. *IEEE Trans. Compon. Parts* **1963**, *10*, 23−30.
(234) Dameron, A. A.; Davidson, S. D.; Burton, B. B.; Carcia, P. F.; McLean, R. S.; George, S. M. Gas Diffusion Barriers on Polymers Using Multilayers Fabricated by Al2O3 and Rapid SiO2 Atomic Layer Deposition. *J. Phys. Chem. C* **2008**, *112*, 4573−4580.
(235) Wu, J.; Fei, F.; Wei, C.; Chen, X.; Nie, S.; Zhang, D.; Su, W.; Cui, Z. Efficient Multi-Barrier Thin Film Encapsulation of OLED Using Alternating Al2O3 and Polymer Layers. *RSC Adv.* **2018**, *8*, 5721−5727.
(236) Malavasi, I.; Bernagozzi, I.; Antonini, C.; Marengo, M. Assessing Durability of Superhydrophobic Surfaces. *Surf. Innovations* **2015**, *3*, 49−60.
(237) Si, Y.; Zhu, H.; Chen, L.; Jiang, T.; Guo, Z. A Multifunctional Transparent Superhydrophobic Gel Nanocoating with Self-Healing Properties. *Chem. Commun.* **2015**, *51*, 16794−16797.
(238) Deng, X.; Mammen, L.; Zhao, Y.; Lellig, P.; Müllen, K.; Li, C.; Butt, H.-J.; Vollmer, D. Transparent, Thermally Stable and Mechanically Robust Superhydrophobic Surfaces Made from Porous Silica Capsules. *Adv. Mater.* **2011**, *23*, 2962−2965.
(239) Wong, W. S. Y.; Stachurski, Z. H.; Nisbet, D. R.; Tricoli, A. Ultra-durable and Transparent Self-Cleaning Surfaces by Large-Scale Self-Assembly of Hierarchical Interpenetrated Polymer Networks. *ACS Appl. Mater. Interfaces* **2016**, *8*, 13615−13623.
(240) Zimmermann, J.; Reifler, F. A.; Schrade, U.; Artus, G. R. J.; Seeger, S. Long Term Environmental Durability of a Superhydrophobic Silicone Nanofilament Coating. *Colloids Surf., A* **2007**, *302*, 234−240.
(241) Yokoi, N.; Manabe, K.; Tenjimbayashi, M.; Shiratori, S. Optically Transparent Superhydrophobic Surfaces with Enhanced Mechanical Abrasion Resistance Enabled by Mesh Structure. *ACS Appl. Mater. Interfaces* **2015**, *7*, 4809−4816.
(242) Gong, D.; Long, J.; Jiang, D.; Fan, P.; Zhang, H.; Li, L.; Zhong, M. Robust and Stable Transparent Superhydrophobic Polydimethylsiloxane Films by Duplicating via a Femtosecond Laser-Ablated Template. *ACS Appl. Mater. Interfaces* **2016**, *8*, 17511−17518.
(243) Tuteja, A.; Choi, W.; Mabry, J. M.; McKinley, G. H.; Cohen, R. E. Robust Omniphobic Surfaces. *Proc. Natl. Acad. Sci. U. S. A.* **2008**, *105*, 18200−18205.
(244) Kota, A. K.; Li, Y.; Mabry, J. M.; Tuteja, A. Hierarchically Structured Superoleophobic Surfaces with Ultralow Contact Angle Hysteresis. *Adv. Mater.* **2012**, *24*, 5838−5843.
(245) Patankar, N. A. Consolidation of Hydrophobic Transition Criteria by Using an Approximate Energy Minimization Approach. *Langmuir* **2010**, *26*, 8941−8945.
(246) Gnanappa, A. K.; Papageorgiou, D. P.; Gogolides, E.; Tserepi, A.; Papathanasiou, A. G.; Boudouvis, A. G. Hierarchical, Plasma Nanotextured, Robust Superamphiphobic Polymeric Surfaces Structurally Stabilized Through a Wetting−Drying Cycle. *Plasma Processes Polym.* **2012**, *9*, 304−315.
(247) Zhu, L.; Shi, P.; Xue, J.; Wang, Y.; Chen, Q.; Ding, J.; Wang, Q. Superhydrophobic Stability of Nanotube Array Surfaces Under Impact and Static Forces. *ACS Appl. Mater. Interfaces* **2014**, *6*, 8073−8079.
(248) Tuvshindorj, U.; Yildirim, A.; Ozturk, F. E.; Bayindir, M. Robust Cassie State of Wetting in Transparent Superhydrophobic Coatings. *ACS Appl. Mater. Interfaces* **2014**, *6*, 9680−9688.
(249) Jung, Y. C.; Bhushan, B. Wetting Transition of Water Droplets on Superhydrophobic Patterned Surfaces. *Scr. Mater.* **2007**, *57*, 1057−1060.
(250) Brown, P. S.; Bhushan, B. Bioinspired, Roughness-Induced, Water and Oil Super-Philic and Super-Phobic Coatings Prepared by Adaptable Layer-By-Layer Technique. *Sci. Rep.* **2015**, *5*, 14030.
(251) Hoshian, S.; Jokinen, V.; Franssila, S. Robust Hybrid Elastomer/metal-Oxide Superhydrophobic Surfaces. *Soft Matter* **2016**, *12*, 6526−6535.
(252) Wang, Y.; Bhushan, B. Wear-resistant and Antismudge Superoleophobic Coating on Polyethylene Terephthalate Substrate Using SiO2 Nanoparticles. *ACS Appl. Mater. Interfaces* **2015**, *7*, 743−755.
(253) Deng, X.; Mammen, L.; Butt, H.-J.; Vollmer, D. Candle Soot as a Template for a Transparent Robust Superamphiphobic Coating. *Science* **2012**, *335*, 67−70.
(254) Bravo, J.; Zhai, L.; Wu, Z.; Cohen, R. E.; Rubner, M. F. Transparent Superhydrophobic Films Based on Silica Nanoparticles. *Langmuir* **2007**, *23*, 7293−7298.
(255) Wong, J. X. H.; Yu, H.-Z. Preparation of Transparent Superhydrophobic Glass Slides: Demonstration of Surface Chemistry Characteristics. *J. Chem. Educ.* **2013**, *90*, 1203−1206.
(256) Xu, L.; Karunakaran, R. G.; Guo, J.; Yang, S. Transparent, Superhydrophobic Surfaces from One-Step Spin Coating of Hydrophobic Nanoparticles. *ACS Appl. Mater. Interfaces* **2012**, *4*, 1118−1125.

https://dx.doi.org/10.1021/acsnano.0c06452
ACS Nano XXXX, XXX, XXX−XXX

(257) Xu, L.; He, J. Fabrication of Highly Transparent Superhydrophobic Coatings from Hollow Silica Nanoparticles. *Langmuir* **2012**, *28*, 7512−7518.
(258) Zhu, X.; Zhang, Z.; Ren, G.; Men, X.; Ge, B.; Zhou, X. Designing Transparent Superamphiphobic Coatings Directed by Carbon Nanotubes. *J. Colloid Interface Sci.* **2014**, *421*, 141−145.
(259) Ebert, D.; Bhushan, B. Transparent, Superhydrophobic, and Wear-Resistant Coatings on Glass and Polymer Substrates Using SiO2, ZnO, and ITO Nanoparticles. *Langmuir* **2012**, *28*, 11391−11399.
(260) Kim, M.; Kim, K.; Lee, N. Y.; Shin, K.; Kim, Y. S. A Simple Fabrication Route to a Highly Transparent Super-Hydrophobic Surface with a Poly(dimethylsiloxane) Coated Flexible Mold. *Chem. Commun.* **2007**, 2237−2239.
(261) Dufour, R.; Perry, G.; Harnois, M.; Coffinier, Y.; Thomy, V.; Senez, V.; Boukherroub, R. From Micro to Nano Reentrant Structures: Hysteresis on Superomniphobic Surfaces. *Colloid Polym. Sci.* **2013**, *291*, 409−415.
(262) Shang, Q.; Zhou, Y. Fabrication of Transparent Superhydrophobic Porous Silica Coating for Self-Cleaning and Anti-Fogging. *Ceram. Int.* **2016**, *42*, 8706−8712.
(263) Verho, T.; Bower, C.; Andrew, P.; Franssila, S.; Ikkala, O.; Ras, R. H. A. Mechanically Durable Superhydrophobic Surfaces. *Adv. Mater.* **2011**, *23*, 673−678.
(264) Aytug, T.; Lupini, A. R.; Jellison, G. E.; Joshi, P. C.; Ivanov, I. H.; Liu, T.; Wang, P.; Menon, R.; Trejo, R. M.; Lara-Curzio, E.; Hunter, S. R.; Simpson, J. T.; Paranthaman, M. P.; Christen, D. K. Monolithic Graded-Refractive-Index Glass-Based Antireflective Coatings: Broadband/omnidirectional Light Harvesting and Self-Cleaning Characteristics. *J. Mater. Chem. C* **2015**, *3*, 5440−5449.
(265) Yuan, Y. C.; Rong, M. Z.; Zhang, M. Q.; Chen, J.; Yang, G. C.; Li, X. M. Self-healing Polymeric Materials Using Epoxy/Mercaptan as the Healant. *Macromolecules* **2008**, *41*, 5197−5202.
(266) Yang, Y.; Urban, M. W. Self-Healing Polymeric Materials. *Chem. Soc. Rev.* **2013**, *42*, 7446−7467.
(267) Wu, D. Y.; Meure, S.; Solomon, D. Self-Healing Polymeric Materials: A Review of Recent Developments. *Prog. Polym. Sci.* **2008**, *33*, 479−522.
(268) Manna, U.; Lynn, D. M. Restoration of Superhydrophobicity in Crushed Polymer Films by Treatment with Water: Self-Healing and Recovery of Damaged Topographic Features Aided by an Unlikely Source. *Adv. Mater.* **2013**, *25*, 5104−5108.
(269) Chen, C.-M.; Yang, S. Directed Water Shedding on High-Aspect-Ratio Shape Memory Polymer Micropillar Arrays. *Adv. Mater.* **2014**, *26*, 1283−1288.
(270) Wang, W.; Salazar, J.; Vahabi, H.; Joshi-Imre, A.; Voit, W. E.; Kota, A. K. Metamorphic Superomniphobic Surfaces. *Adv. Mater.* **2017**, *29*, 1700295.
(271) Xue, C.-H.; Bai, X.; Jia, S.-T. Robust, Self-Healing Superhydrophobic Fabrics Prepared by One-Step Coating of PDMS and Octadecylamine. *Sci. Rep.* **2016**, *6*, 27262.
(272) Neinhuis, C.; Koch, K.; Barthlott, W. Movement and Regeneration of Epicuticular Waxes Through Plant Cuticles. *Planta* **2001**, *213*, 427−434.

https://dx.doi.org/10.1021/acsnano.0c06452
ACS Nano XXXX, XXX, XXX−XXX